NRL Memorandum Report 4284
EOTPO Report 62

Reduction and Assessment of Infrared Background Data

SCOTT M. SINGER, FREDERICK G. SMITH, TIMOTHY J. ROGNE

OptiMetrics, Inc.
2000 Hogback Road, Suite 3
Ann Arbor, Michigan 48104

RICHARD A. STEINBERG

Electro-Optical Systems Development Group
Optical Sciences Division

August 7, 1980

ELECTRO-OPTICAL TECHNOLOGY PROGRAM OFFICE
NAVAL RESEARCH LABORATORY
Washington, D.C.

Reviewed and Approved by

Dr. John M. MacCallum, Jr.

Head, Electro-Optical Technology Program Office

Naval Research Laboratory, Washington, D.C. 20375

SECURITY CLASSIFICATION OF THIS PAGE (When Data Entered)

REPORT DOCUMENTATION PAGE

READ INSTRUCTIONS BEFORE COMPLETING FORM

1. REPORT NUMBER: NRL Memorandum Report 4284	2. GOVT ACCESSION NO.: AD88 247
3. RECIPIENT'S CATALOG NUMBER:	
4. TITLE (and Subtitle): REDUCTION AND ASSESSMENT OF INFRARED BACKGROUND DATA	5. TYPE OF REPORT & PERIOD COVERED: Interim report on a continuing NRL problem
	6. PERFORMING ORG. REPORT NUMBER: OMI-80-002 EOTPO Report 62
7. AUTHOR(s): Scott M. Singer†, Frederick G. Smith†, Timothy J. Rogne† and Richard A. Steinberg	8. CONTRACT OR GRANT NUMBER(s): N0014-79-C-0461
9. PERFORMING ORGANIZATION NAME AND ADDRESS: OptiMetrics, Inc., 2000 Hogback Road, Suite 3, Ann Arbor, Michigan 48104	10. PROGRAM ELEMENT, PROJECT, TASK AREA & WORK UNIT NUMBERS: 62332N; ZF32-391-003
11. CONTROLLING OFFICE NAME AND ADDRESS: Naval Research Laboratory, Washington, D.C. 20375	12. REPORT DATE: August 7, 1980 13. NUMBER OF PAGES: 74
14. MONITORING AGENCY NAME & ADDRESS (if different from Controlling Office): NRL; NRL/EOTPO	15. SECURITY CLASS. (of this report): UNCLASSIFIED
	15a. DECLASSIFICATION/DOWNGRADING SCHEDULE

16. DISTRIBUTION STATEMENT (of this Report)

Approved for public release; distribution unlimited.

DTIC ELECTE AUG 20 1980 S D B

17. DISTRIBUTION STATEMENT (of the abstract entered in Block 20, if different from Report)

18. SUPPLEMENTARY NOTES

†Present address: OptiMetrics, Inc., 2000 Hogback Road, Suite 3, Ann Arbor, Michigan 48104

19. KEY WORDS (Continue on reverse side if necessary and identify by block number)

Infrared technology
Electro-optical technology program office (EOTPO)
Electro-optics
Infrared signatures

20. ABSTRACT (Continue on reverse side if necessary and identify by block number)

The outstanding problem in designing passive infrared detection sensors is the design of effective target/background discrimination algorithms. A key factor in the design process is the requirement for a data base of high spatial resolution, low noise, background imagery. The cloud and ocean sunglitter data discussed in this report, obtained by Cincinnati Electronics Co. (CECO), are intended to help satisfy this requirement for infrared (IR) background imagery. We recommend that future IR backgrounds measurements with the CECO radiometer incorporate the following suggestions: the CECO radiometer should be upgraded to incorporate DC restoration; data should

(Abstract continues)

DD FORM 1 JAN 73 1473 EDITION OF 1 NOV 65 IS OBSOLETE
S/N 0102-LF-014-6601

SECURITY CLASSIFICATION OF THIS PAGE (When Data Entered)

(Abstract continued)

20. be recorded from all 24 detector channels, rather than just 8 channels; tape recorder noise should be decreased by improving the data recording system.

CONTENTS

REDUCTION AND ASSESSMENT OF INFRARED BACKGROUND DATA

1
INTRODUCTION

The outstanding problem in designing passive infrared (IR) detection sensors is the development of effective target/background discrimination algorithms. To address this problem video data obtained from actual backgrounds must be recorded and played back against a variety of algorithms. An iterative approach of algorithm modification/performance evaluation then leads to an evolving family of ever-improving signal processor designs.

A key factor in the design process is the requirement for a data base of high spatial resolution, low noise, IR background imagery. The data discussed in this report are intended to help satisfy this requirement for IR background imagery, as a necessary antecedent to the sound design of autonomous IR target acquisition sensors.

Section Two presents a general overview of the background measurements program. Included are brief descriptions of the data collection procedures, the instrumentation used, and the data available for analysis. Section Three describes in detail the data reduction procedures employed to digitize the analog data. Section Four contains a complete description of the available digital data including an assessment of the data quality. Section Five presents the results of a preliminary analysis of the data. Section Six draws conclusions and presents recommendations for further work.

A description of the Key West test site, additional detail on the Cincinnati Electronics Co. (CECO) radiometer, and photographs of the visual scenes corresponding to the IR background signatures may be found in Reference 1.

Manuscript submitted June 6, 1980

2
BACKGROUND

The CECO measurements were obtained during the first two weeks of May 1979 in the Florida Keys with the MIDAS III sensor system. The specifications of the instrument configuration used to obtain the data are given in Figure 1. Although 8 - 13 μm measurements were also made, this work only addresses the 3 - 5 μm data currently made available for analysis by CECO.

The data are obtained by sweeping a vertical, eight-detector array horizontally through the focal plane of the instrument. Each sweep maps the radiance of a 0.76 x 28 mrad section of the sky. The signal from each detector is recorded on a separate track of an analog tape recorder along with a synchronization signal, a timing signal and a voice track. A description of the tape recorder is presented in Figure 2. The system relative spectral response curves (radiometer plus filter) for each of the 3 - 5 μm wavebands are given in Appendix A, as obtained from Reference 1.

In the recent tests, the instrument was operated as follows. First, the instrument was pointed in the general direction of a visually structured background scene. Next, the instrument output was viewed on an oscilloscope and a minor instrument-pointing adjustment was made to locate a relatively highly structured area e.g., a cloud edge. Several seconds of data were then accumulated for each spectral bandpass (filter). The typical sampling gave 10 seconds of data in each band, with 40 seconds required for a complete cycle through the various filters. Auxiliary information was recorded on the voice track and

NEI (w/cm^2) (approximate)	2×10^{-14}
TOTAL FOV (mrad)	28 x 0.76 (az x el)
INSTANTANEOUS FOV (mrad)	0.095 x 0.114 (az x el)
FRAME RATE (sec^{-1})	10
DWELL TIME (ms)	0.254
CHANNELS RECORDED	8
ELECTRONIC BANDWIDTH (Hz)	0.05 - 1900 (-3 dB)
SPECTRAL BANDPASS (μm)	3.0 - 5.1 (Filter #1) 4.4 - 4.8 (Filter #2) 3.8 - 4.2 (Filter #5) 3.4 - 4.3 (Filter #6)
APERTURE (inches)	7
FOCAL LENGTH (inches)	21
FRAME TIME (ms)	75
RETRACE TIME (ms)	25

Fig. 1 — Midas instrument specifications

ANALOG INSTRUMENTATION RECORDER	Ampex Model FR-13
CHANNEL IDENTIFICATIONS	#1 - 8 Data #12 IRIG Time #13 Azimuth Sync #14 Voice
CHANNEL DELAYS	1.25 ms for odd with respect to even
TAPE SPEED	7.5 ips
AMPLIFIER SPECIFICATION	Intermediate band, 13.5 KHz carrier, 2.5 KHz bandwidth
NOMINAL RECORDER S/N	38 dB with respect to full scale

Fig. 2 — Data recording specifications

in a data log. In all, 58 such data sets were recorded. These consisted primarily of cloud or sky data, but they also included a few scans of terrain and solar glitter from the ocean. Scans of a constant temperature blackbody were also taken periodically during the measurements. Polaroid photographs were taken of most scenes and 35 mm telephoto photographs of the FOV were taken for certain scenes.

The MIDAS III detectors are AC coupled with a 0.05 Hz cut-on frequency. Therefore, the irradiance data are not absolute. On the other hand, the cut-on frequency is sufficiently low that a single scan shows no "droop" across the total FOV. Because the spectral filter is not instantaneously changed and the electrical response requires time to settle after each filter change, several frames of data are compromised following a filter change. Thus, band-to-band comparisons of a single scene can be done with a time lag of no less than about 0.2 seconds. Thus, it generally is only possible to make direct comparison between spectral bands which are adjacent in the data acquisition sequence. However, qualitative comparisons of the spatial variability of the background about the mean radiance level can be made for all spectral bands.

3
DATA REDUCTION

This section describes the procedures and equipment used to convert the analog data supplied by CECO to a digital form suitable for analysis. The flow chart in Figure 3 outlines the data reduction process. The analog data for selected scenes are fed through a signal conditioning unit to an analog-to-digital (A-D) converter controlled by a minicomputer. The raw digital data produced by the A-D converter, initially stored on a disk drive, are transferred to a digital magnetic tape at the conclusion of each scene. These tapes are then read by a main-frame computer which performs all post-processing of the raw digital data for selected scans. The radiant exitance data so obtained are then written on a tape for later analysis. This process is described in detail in the following subsections.

3.1 DIGITIZATION

Eight analog signals corresponding to the eight detector positions on the instrument array were recorded for each of 58 background scenes. In addition, a synchronization signal was recorded which identifies the scan and retrace modes of the instrument. Filter-wheel position was encoded on the retrace pulse. A timing signal coded in the IRIG B format was also recorded as was a signal containing a running verbal commentary on the test series. All signals were FM recorded except for the voice and time signals which were directly recorded.

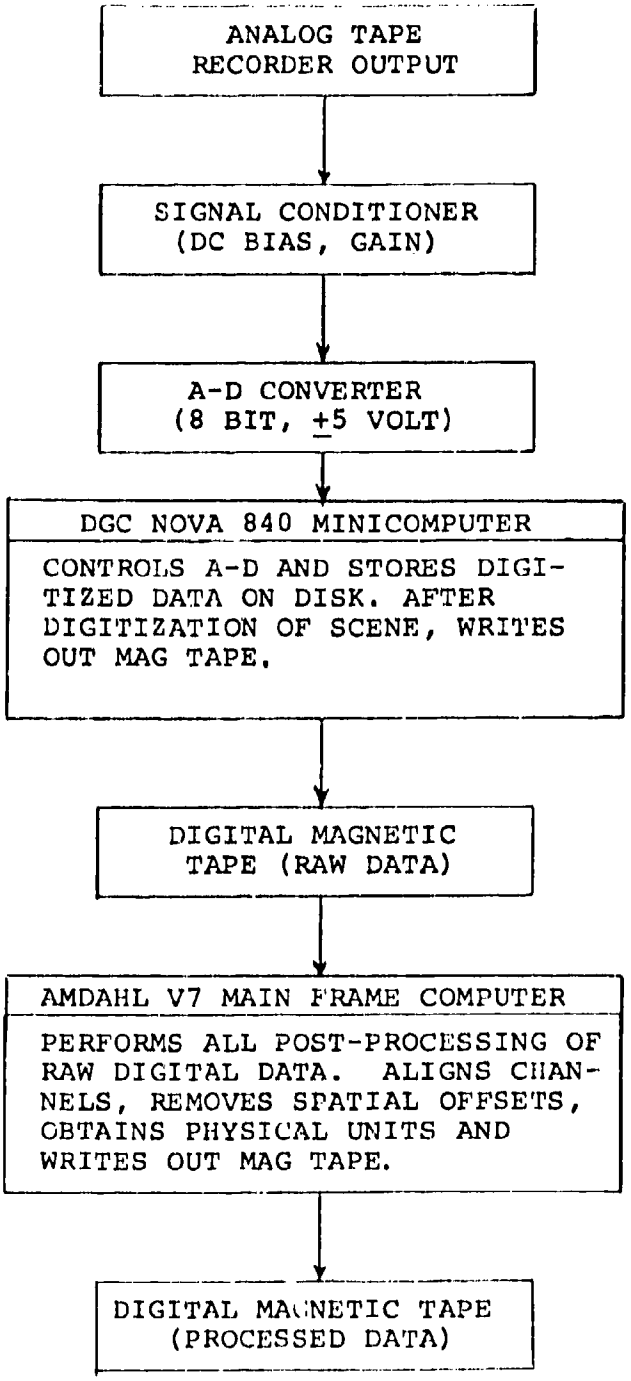

Fig. 3 — Data reduction flow chart

An AMPEX Model CP-100 analog instrumentation recorder was used to reproduce the eleven data channels just described. While this recorder is older than the FR-13 used to record the data, the two recorders have identical bandwidth and signal-to-noise characteristics. The CP-100 was calibrated and tested prior to the data reduction. AC and DC test signals were recorded and their reproduction was found to be well within the manufacturer's specifications. Following the data reduction, similar testing verified that the tape recorder performance was unchanged.

Optimally, it is desirable to digitize all eight data channels, the sync and the timing channels, simultaneously. This was not possible, however, due to constraints of sampling frequency, data storage, and available electronic hardware (tape recorder amplifiers, signal conditioner amplifiers, and A-D sample-and-hold circuitry).

The MIDAS III data were digitized at a 3 KHz sampling rate. This choice was both convenient in terms of the electronic hardware available, and sensible in terms of recovering the information available in the analog data.

Determination of a digitization rate often involves a complex trade-off analysis, but it can be estimated directly by computing the analog data bandwidth. This, in turn, is determined by the measurement system's Modulation Transfer Function (MTF).

Assuming the MIDAS III MTF to be composed of an aperture, electronic (video) and tape recorder response, one can integrate the component responses to obtain an equivalent bandwidth, Δf, for the system:

$$\Delta f = \int_0^\infty H^2(f)_{\text{aperture}} \, H^2(f)_{\text{electronic}} \, H^2(f)_{\text{tape}} \, df$$

Approximating the aperture response by the sinc function and the electronic and tape recorder responses by single pole filters with 3 dB points at 1900 Hz and 3000 Hz, respectively, we have;

$$\Delta f = \frac{1}{\pi t_o} \int_0^\infty \left(\frac{\sin^2\alpha}{\alpha^2}\right)\left(\frac{1}{1 + (\frac{\alpha}{\alpha_e})^2}\right)\left(\frac{1}{1 + (\frac{\alpha}{\alpha_t})^2}\right) d\alpha$$

where t_o = instrument dwell time ≈ 0.254 ms

$\alpha = \pi t_o f$

$\alpha_e = 0.48\pi$

$\alpha_t = 0.76\pi$

Evaluating the above integral yields an equivalent bandwidth of 1200 Hz. In other words, we could recover all the available spectral information by sampling at the Nyquist frequency of 2400 Hz, assuming the MIDAS III instrument response to be that of an ideal low-pass filter. The 3 KHz sampling rate chosen for this study reflects the fact that the data contain signal frequencies greater than 1200 Hz, though these signals have been attenuated by the instrument response. A 3 KHz sampling rate permits detection of signal frequencies less than 1500 Hz. The signal energy at 1500 Hz has been attenuated by roughly a factor of 3 by the instrument response.

In actuality, the instrument attenuation is probably much greater than that. The MTF of the optics and detector have been ignored here for simplicity. The nominal single-pole filters used to estimate the electronic and tape recorder response are more realistically multiple-pole filters, i.e., filters having a sharper cut-off. The effects of the signal conditioner and the A-D converter have not been included. All of these factors reduce the bandwidth even further.

In order to accurately reconstruct the signal energies which have been seriously degraded by the total instrument response, one must very accurately specify the MTF of the system. However, even this is not sufficient if the noise has been inserted following the primary signal apertures. The tape noise is the principal noise source in this case (refer to Table 6) and is not attenuated by the video electronics at all. Thus, the signal-to-noise ratio at some critical frequency may be such that an attempt to reconstruct the signal only yields a noise spectrum.

Given all these considerations, the 3 KHz sampling rate appears to be a good compromise.

Four channels (two data channels, sync and timing channel) are digitized simultaneously at the 3 KHz rate (12000 datum points/second/four channels) for each scene. Four separate passes are made through the scene to digitize all eight data channels. Data are sampled continuously for approximately one minute (704800 datum points/scene/four channels).

All four signals to be digitized are passed through a signal conditioning unit. This unit has both gain and DC bias adjustments. Though the radiometric data were AC coupled before being recorded, negative DC biases as large as -0.8 volts were noted when the data were reproduced. These become quite significant as gain is applied to the signals. The A-D converter produces an 8-bit, ± 5 volt output (LSB = 39 millivolts). The recorded signal amplitude ranged from 50 millivolts to nearly a volt, well above the 12 millivolt noise level of the tape recorder. However, to take full

advantage of the dynamic range of the A-D converter, it is clearly necessary to apply a gain to the signal and at the same time counteract the effects of the recorded DC biases, thus preventing saturation. The signal conditioning unit performed that function.

Two nominal gain settings are used in the digitization. A gain of five was used for the two sea glitter scenes and a gain of ten was used for all others. An electronic calibration signal (1.0v peak-to-peak, 1 KHz, sine wave) was recorded at three times during the data taking sequence. The first of these is digitized and the actual system gain is accuratley computed from those data. To relate that calibration signal to subsequent calibration signals, an integrating voltmeter is used to measure the RMS voltages of the respective signals. The resulting ratios are applied to the originally computed gain to obtain the other gain factors.

The gain was kept below the value ($\sim$10) for which the calibration signal would saturate the A-D converter. (If the data had not been tape-noise-limited, it might have been desirable to use gain factors greater than ten for the smaller signals in order to decrease A-D noise relative to tape and detector noise.) The calibration signal is digitized both before and after all the scene data for a particular data channel pair are digitized. This serves as a useful check on our digitization procedures by ensuring that the electronics in the tape recorder, signal conditioning unit, and A-D converter remain stable throughout.

The digitization proceeds under the direct control of a Data General Corporation Nova 840 minicomputer. The operator need only signal the computer when to begin digitization. He does this by visually monitoring the data channels on an oscilloscope and listening to the recorder voice track. Following digitization of a particular scene, the data, coded as 16-bit, two's complement, binary integers, are written out onto a digital magnetic

tape for later use in the post-processing phase of the data reduction.

3.2 POST-PROCESSING

As a result of the piece-wise digitization technique described above, the four data sets which comprise one complete scene are temporally misaligned with respect to one another. This misalignment must be corrected before single scans may be extracted within a scene.

The original intention at this stage was to use the timing signal to realign the data. However, the timing signal was not recorded for four of the scenes selected for analysis. An alternate methodology was developed which utilized the filter identifier encoded on the sync signal. A computer program was written which scanned the data and counted the number of scans for each filter position. Whenever the filter number changed, the program printed the number of scans for the last filter and the sequential position within the file where the first scan with that filter began. By visually comparing the patterns so generated for all four data sets, it is possible then to compute a corrective offset which aligns the data within an accuracy of one datum sample.

After applying the above methodology, certain problems became evident. First, the average number of datum points comprising one scan varied significantly from scene to scene. Second, the even channels were offset with respect to the odd channels by an invariant, but large amount. A small offset is expected resulting from the sensor's detector geometry, but the measured offset was an order of magnitude larger.

The first problem is thought to result from tape recorder speed fluctuations at the time the original

data were recorded. The piece-wise digitization procedure bears this out. If either the tape recorder speed or the A-D converter sampling frequency varied during playback, the number of datum samples within one scan is expected to be different for the four different data channel pairs simply because they are digitized far apart in time. Table 1 illustrates that this was not the case. With the exception of Scene 5, the average number of samples/scan is essentially constant within a given scene irrespective of the data channel. The sync channel for Scene 5 was peculiarly noisy and that probably accounts for the small variation observed with data channel. However, between scenes the average number of samples/scan varies significantly, ranging from 218 (Scene 5) to 167 (Scene 35). Table 2 presents the number of samples/scan as a function of filter sequence and scene for a particular data channel pair. This shows that the speed was varying up to $\pm 3\%$ within the scenes themselves, as well.

A change in tape speed is equivalent to modulating the FM carrier frequency and produces a DC voltage output in direct proportion to that change. This may account for the DC offsets which were noted during the digitization. These changes in speed affect the data quality in two ways.

First, if the changes occur on the order of the seventy-five millisec scan time, a $\pm 1\%$ speed modulation corresponds to a ± 35 millivolt signal modulation. Combine that with a typical signal level of ± 25 millivolts and it is obvious that the data will be seriously distorted. Specifically, an artificial low-frequency spatial modulation is introduced. If the speed changes occur more slowly, the only effect is to introduce a DC

TABLE 1. AVERAGE NUMBER OF SAMPLED POINTS/SCAN AS A FUNCTION OF DATA CHANNEL AND SCENE FOR LAST FILTER IN SEQUENCE

	DATA CHANNEL #			
SCENE #	2,4	6,8	1,3	5,7
5	217	218	215	213
8	200	200	199	199
11	199	198	198	198
18	176	174	174	174
28	189	189	189	189
31	176	176	177	176
35	167	167	167	167
42	184	184	184	184
57	207	207	207	207

TABLE 2. AVERAGE NUMBER OF SAMPLED POINTS/SCAN AS A FUNCTION OF FILTER SEQUENCE AND SCENE FOR DATA CHANNELS 2,4

	FILTER SEQUENCE #			
SCENE #	1	2	3	4
5	214	213	214	217
8	202	203	199	200
11	200	199	199	199
18	178	175	177	176
28	185	186	184	189
31	170	175	180	176
35	171	168	170	167
42	190	189	181	184
57	203	204	206	207

level. This is of no consequence as the data are not intended to be absolute. Second, variations in tape speed directly impact the effective sampling rate and thus, the highest spatial frequencies which can be resolved. The sampling rate referenced to real-time was indeed 3000 Hz. This is equivalent to sampling 225 datum points in a 75 millisec scan. As shown in Tables 1 and 2, the actual number of points/scan was typically some 3%-25% less than expected. High spatial frequency data are therefore aliased. Without a priori knowledge of the true spectral content of a scene, it is not possible to immediately assess this effect.

The offset of the even channels with respect to the odd channels is hypothesized to result from an apparent slight spacing difference of the tape reproduce heads with respect to the tape record heads. On most 14-channel analog instrumentation tape recorders, the record and reproduce head assemblies are each composed of two stacks. Each stack has seven channels either all odd or all even. A difference of only 0.15 cm in spacing between the odd and even tape heads is sufficient to account for the delay observed. This was corrected by selecting a prominent feature in one of the scenes (a microwave tower) and offsetting the even channels to align with the odd. The odd were correct since the sync pulse was itself recorded on an odd channel. Fortunately, a single offset correction (23 datum points) is sufficient as the tape recorder speed was invariant while digitizing the data.

Four complete scans have been digitized for each of eight channels for each of four filters for each of nine scenes. The scans were arbitrarily chosen to be the 11th - 14th scan following a change of filter. This ten-scan waiting interval before data extraction was not nearly long enough to allow the transient response of the AC coupler to decay. Thus, we have a second possible

explanation for the observed DC offsets in the data.

To facilitate the processing of the data, the datum points in each scan are linearly interpolated to a 0.1 mrad interval scan grid. This produced scan records of a constant length (281 points) thus eliminating the effects of varying tape speed (varying sampling interval). Note that no improvement in spatial resolution results or should be inferred from this apparent expansion of the data records.

The scan data are biased to zero their mean value and the system gain corrections are applied. The data are converted to voltages and the calibration factors presented in Table 3 are applied to convert the datum points to radiant exitance values (watt/cm^2). The detector geometry introduces a small delay of 1.25 millisec between the odd and even channels. This is corrected by shifting the odd channel data 5 positions ($\sim$0.47 mrad). Note that the last five data values for all the odd channels are set to the value of 9999 to indicate that the values are missing. The processed data are then formatted and written onto a magnetic tape for future analysis.

TABLE 3. MIDAS III CALIBRATION FACTORS

SPECTRAL BAND	FILTER #	CALIBRATION FACTOR (10^{-3} w/cm^2/volt)
3.0 - 5.1 μm	1	1.63
4.4 - 4.77 μm	2	1.21
3.8 - 4.2 μm	5	1.76
3.4 - 4.3 μm	6	1.62

4
DESCRIPTION OF DIGITAL DATA

4.1 DATA AVAILABLE

Processed digital radiant exitance data are available on tape for the nine scenes listed in Table 4. A total of 128 scans are included for each scene (4 scans/ 8 data channels/4 spectral filters).

Unprocessed digitized data are available on tape for all scenes listed in Table 4. These tapes contain the complete data record for each scene. Should additional processing be desired, the software currently exists to extract such data.

4.2 DATA FORMAT

The processed data are supplied on a digital magnetic tape. Each scan consists of thirty-seven card image records. Record 1 is a header containing scene #, filter #, channel #, and scan #. Records 2-37 contain 281 radiant exitance values in order of azimuthal position. These correspond to positions 0-28 mrad at intervals of 0.1 mrad. This information is summarized in Table 5. Missing datum values are coded as 9999. Note that the last five values are always missing for the odd channel scans due to the detector geometry. The scans are ordered on the tape as indicated in Figure 4 and the tape is formatted as follows:

- 9 track digital magnetic tape
- unlabelled
- 1600 bpi
- EBCDIC
- card image (80 characters/record)
- blocked (100 records/block)

TABLE 4. BACKGROUND SCENES SELECTED FOR ANALYSIS
(Reference 1)

SCENE	DESCRIPTION	DATE/TIME MAY 1979	ELEVATION (degrees)	LOS AZIMUTH (degrees)	SUN-TO-LOS ASPECT (degrees)	TEMP (°F)	RH (%)
5	Ocean sun glitter	2/0947	-0.45	86	86	81	65
8	Cumulus cloud	2/1025	10.3	90	47	81	62
11	Cloud	3/1015	7.2	120	52	81	65
18	Cloud	4/0937	3.8	82			
28	Cloud	4/1542	9.1	308	58	82	58
31*	Microwave tower against sky	5/0910	1.0	108	45	81	62
35	Cloud	5/1015	9.46	103	46	83	60
42*	Fluffy clouds near horizon	8/1035	2.1	66	87	82	69
57	Cloud edge against sky	10/0932	11.4	114	108	84	55

LOS - sensor line-of-sight
RH - relative humidity
Visibility > 7 statute miles for all measurements
Cloud scenes 28 and 35 were tracked with the radiometer; all other scenes were recorded with radiometer stationary.
All measurements obtained at Key West, Florida (lat. 24°33.1'N, Long. 81°, 47.8'W).
* Low elevation data (Scenes 31 and 42) were largely dominated by tape noise.

TABLE 5. DATA RECORD FORMAT

# RECORDS	RECORD TYPE	DATA	FORTRAN FORMAT
1	Header	Scene # Filter # Channel # Scan #	(4I5)
36	Data	281 Radiant Exitance Values	(8E10.4)

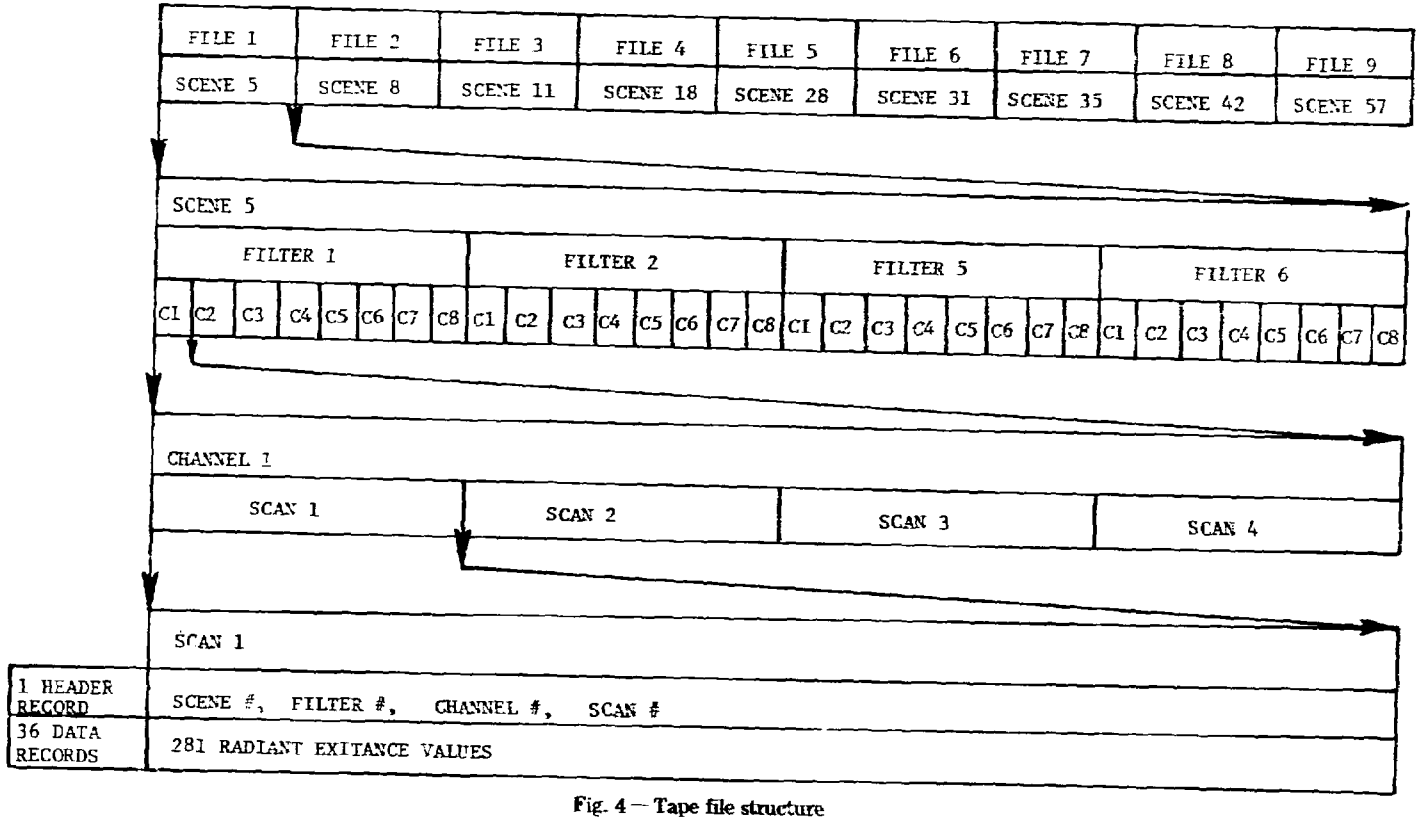

Fig. 4 — Tape file structure

4.3 DATA QUALITY

The quality of the processed data suffers as a result of three principal problems. In order of importance, these are (1) the suspected tape recorder speed fluctuations discussed in detail in Section 3.2, (2) the apparent calibration signal amplitude variations, and (3) the limited number of recorded calibration and blackbody signals.

The tape recorder speed problem manifests itself in two ways. First, the high frequency spatial content of a scene has been attenuated and the energy aliased into lower frequencies. This results from the effective sampling rate being decreased by as much as 25% by the tape speed variations. Note that the variations are inherent in the recorded data, and are not artifacts of the data reduction procedures. The extent of the signal distortion can be assessed by digitizing a scene at progressively higher rates and comparing the results.

Second, spatial frequency components may have been artifically inserted into the data as a result of the speed variations. The degree of distortion produced in such a case depends only on the relative speed at which the tape speed modulation occurs. To assess the magnitude of this effect, the Ampex FR-13 tape recorder needs to be thoroughly tested. The results would be fairly conclusive assuming no adjustments have been made to the machine in the interim.

As discussed in Section 3.1, an electronic calibration signal was recorded periodically so that the gain of the system could be determined. These signals exhibited curious short and long-term fluctuations. The computed system gains increased for all data channels from the initial to the final calibrations. Certain of these

increases exceeded 20%. It is our understanding that the detector gains are fixed. Thus, the source of such a long-term gain change is not clear. Instabilities in the tape recorder amplifiers are one possibility. The calibrations themselves are typically 30 seconds in length. Within that short time span, variations in amplitude of $\pm$3% were noted. This is highly unusual behavior. The conclusion to be drawn from the evidence presented here is that the gains may have been changing from scene to scene and perhaps within scenes. This in itself does not impact the data quality unless the rate at which the gains changed was faster than the frequency of recorded calibration signals.

The test series spanned some ten days. During that period only three calibration signals were tape recorded. It is clear from the above discussion that the accuracy of the data may be compromised by the infrequent calibrations. However, the magnitude of this effect cannot be determined after the fact.

Only one series of scans of a reference blackbody source was recorded. As there was no filter number encoded on the sync pulse, it was not possible to reduce those data to physical units. Later testing by CECO also disclosed that the reference source employed was not a satisfactory blackbody.

The data collection sequence limits the use of these data. Direct spectral comparisons are often not meaningful because the data were collected for ten seconds for each of four filters. The time between filters one and six is thus 20 seconds at best. Cloud position can change significantly in such a period, as borne out by the data. However, scans could be extracted near the end of one filter's

data and at the beginning of the next. Their temporal proximity would facilitate such comparisons if only for spectral band pairs.

5
DATA ASSESSMENT

The principal results of this program are the digitized exitance values which were provided to NRL on magnetic tape as described in Section 4. In addition, a brief examination was made of the physical validity of the data and some interesting features were noted.

5.1 CLOUD SCENES

A simple cloud radiance model was used to obtain a confirmation of the magnitude of the measured results. The "theoretical" model used was suggested by Maxwell and Lindquist [2] and is illustrated in Figure 5. The model assumes that the cloud radiance can be represented as the sum of a diffuse solar scattered component plus a gray-body thermal emission component. These two components are represented by the dashed and dotted curves in the figure assuming a diffuse reflectivity of 0.8 and a 300K graybody with an emissivity of 0.2. The sum of these components, modified by an approximate atmospheric transmittance, is shown by the solid curve in the figure.

The results of the cloud radiance model were averaged over the spectral bands of the measurements (assuming a rectangular bandpass) and plotted as in Figure 6. There, each spectral average is represented by a solid horizontal line at the averaged ordinate value with endpoints at the band edges. Thus, Figure 6 compactly illustrates the "expected" radiant exitance values for the various bands.

Average radiant exitance values were obtained for two scenes which appeared to include cloud edges, for comparison with the "theoretical" values. To facilitate comparison between the available model and the CECO data, we assumed that the

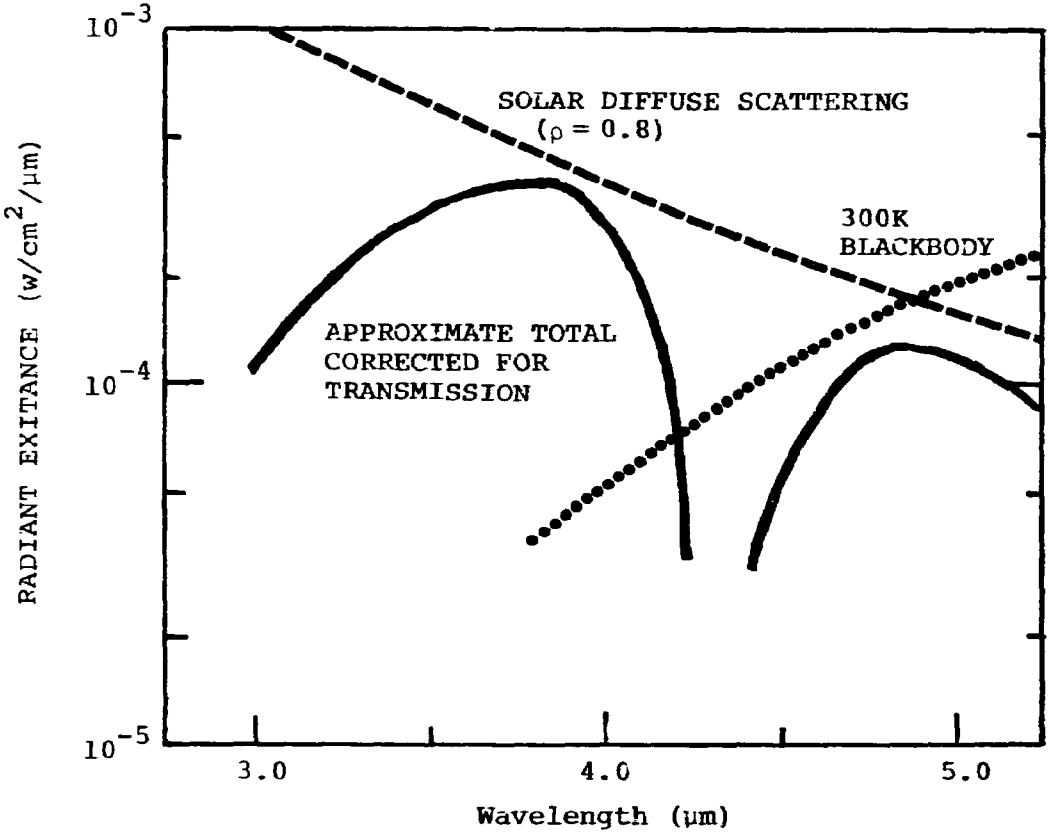

Fig. 5 — Theoretical radiant exitance as a function of wavelength. (Obtained from Ref. 2)

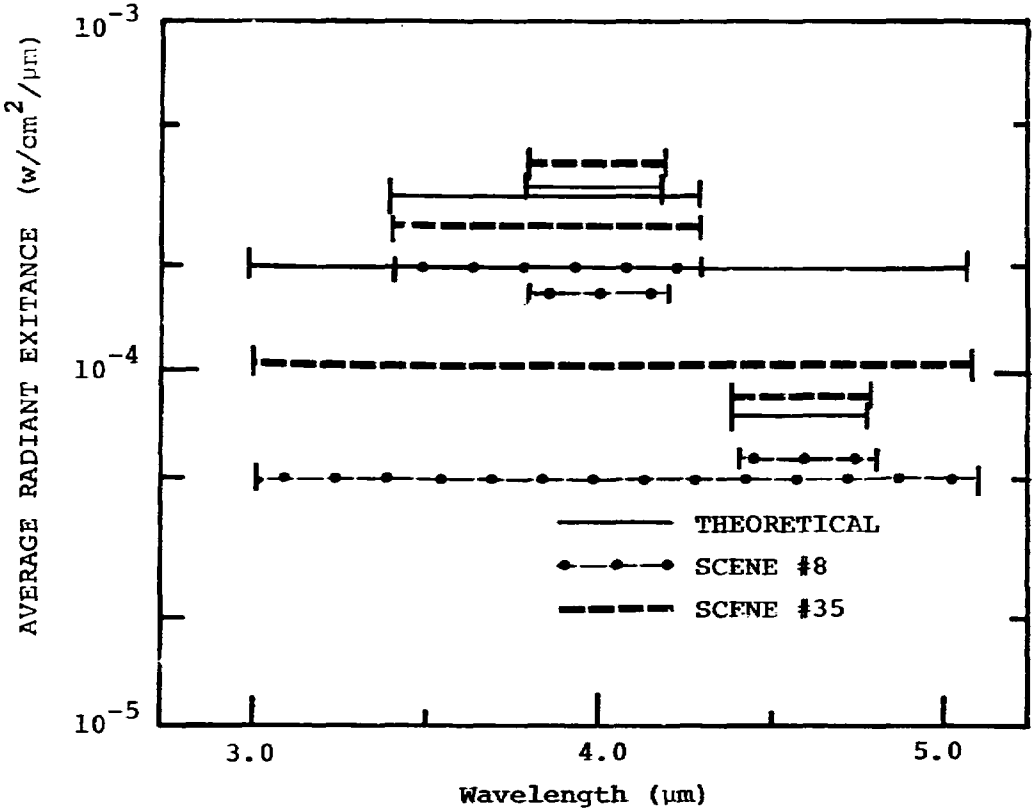

Fig. 6 — Comparison of measured band-averaged radiant exitance values with theoretical approximations as a function of bandpass.

blue sky provided a low radiance background and hence that the measured cloud radiant exitance values can be directly compared with the predicted values. The resulting comparisons are shown in Fig. 6. Note, however, that in Fig. 6 we have compared theoretical cloud absolute radiance with measured cloud/sky contrast. Perhaps model and measurements would have been in better agreement if either the CECO data were DC-restored, or if the model were modified to generate cloud/sky contrast.

Unfortunately, detailed comparison of the various spectral bands is difficult with the present data set because of the time interval which separates the spectral data. It is clear that in many cases the scene was changing rapidly during the measurements. This is illustrated in Figure 7 which apparently shows the cloud edge moving through the instrument's field-of-view during sequencing of the spectral bandpass filters. Even in this figure, however, features of the cloud scene are identifiable from filter to filter. This was not generally true of the weaker cloud radiance scenes as illustrated by Scene 42 in Figure 8. Through inspection of the latter figure, it is difficult to unambiguously identify even one feature of the scene which persists from band to band. Although the radiant exitance variations observed in this scene are comparable in magnitude to the tape recorder noise, inspection of adjacent channels and subsequent scans indicate that much of the structure is real. However, this is a case where the data acquisition system has seriously affected the data quality.

We note that by integrating the sky/cloud spectral signature in Reference 3 from 3.2 - 4.8 μm, a peak contrast exitance $\sim 2.5 \times 10^{-4}$ w · cm^{-2} is obtained. This is very nearly equal to that obtained from the CECO data (Scene 35).

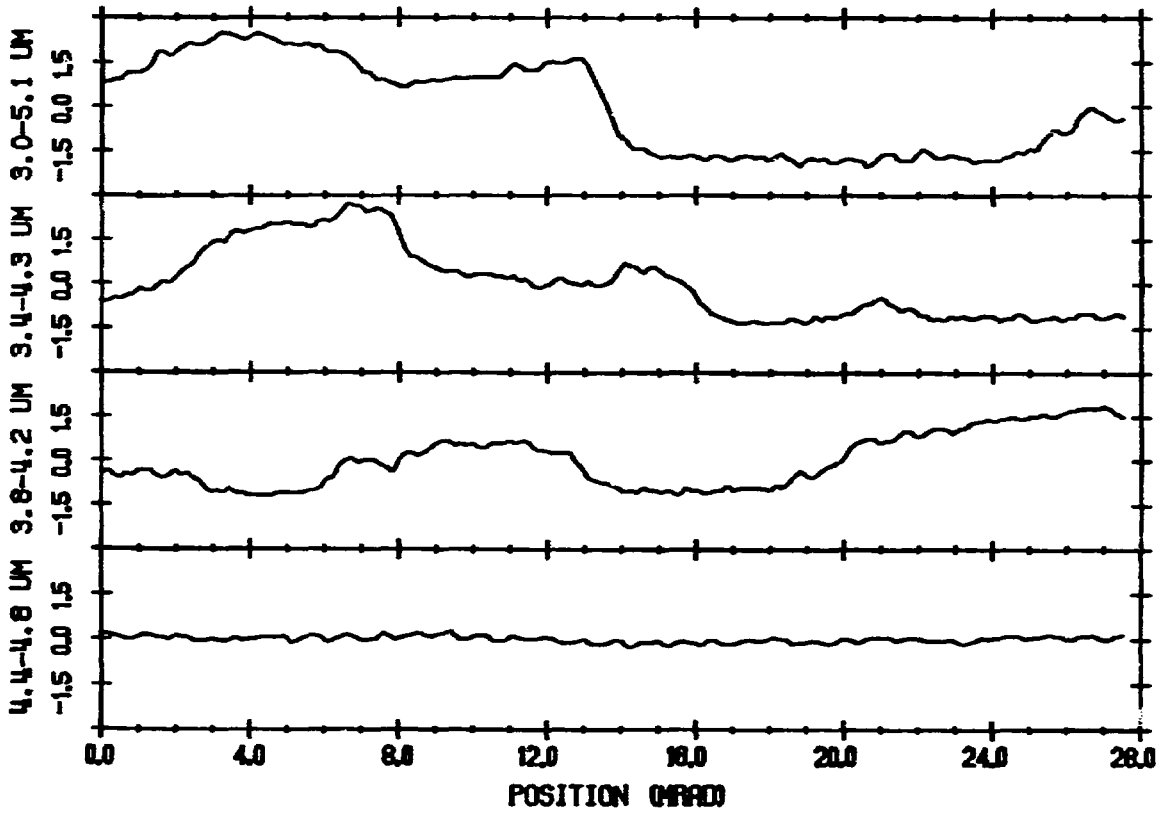

Fig. 7 — Radiant exitance (10^{-4} w/cm^2) presented as a function of spectral bandpass for scene #35 (cloud), Scan #1, Channel #1.

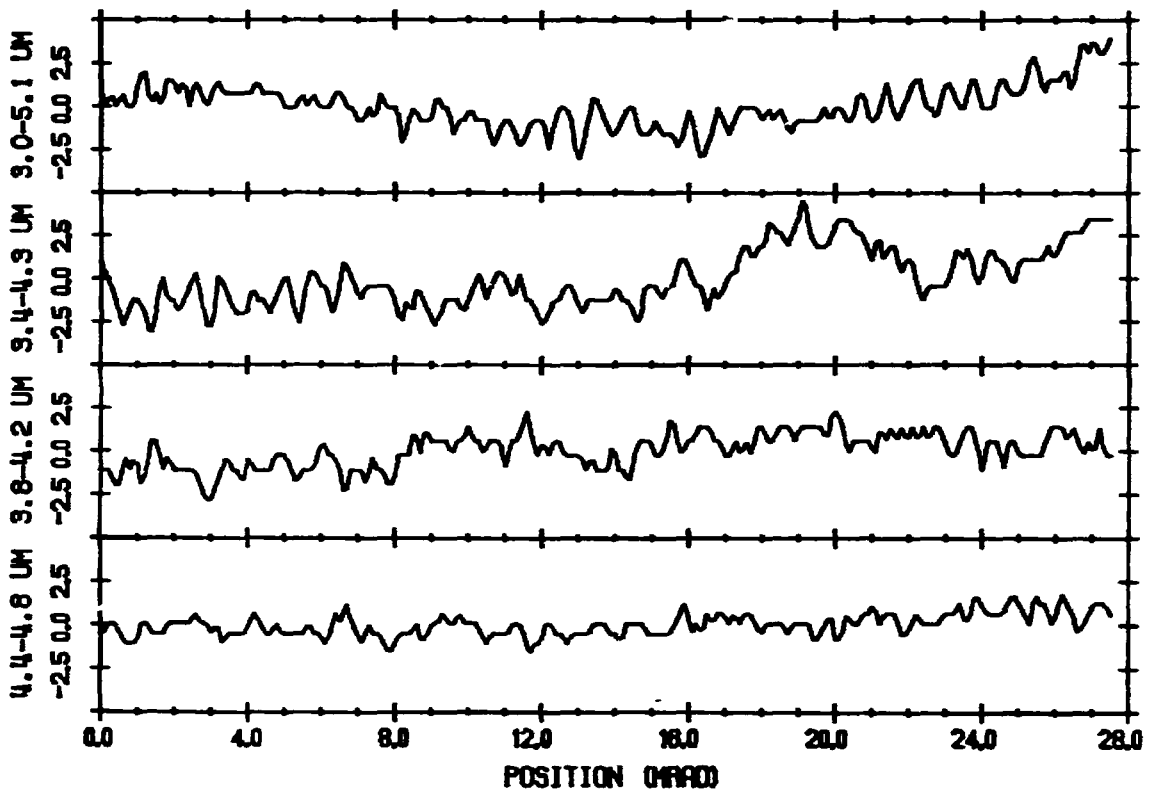

Fig. 8 — Radiant exitance (10^{-5} w/cm^2) presented as a function of spectral bandpass for scene #42 (cloud deck near horizon), Scan #1, Channel #1. Data are largely dominated by tape noise (cf. Table 6).

5.2 OCEAN SUN-GLINT SCENES

We have not performed a detailed analysis of the sunglint scenes at present. However, it is interesting to note some of the more obvious features of these data. Figure 9 shows one example of the sea glitter results. Each of the eight detector signals is represented as a function of the field-of-view position indicated on the horizontal scale. One notable feature is the intensity of the signal levels, $\sim 10^{-3}$ w/cm^2, which is roughly an order of magnitude greater than the most intense cloud scenes.

Another notable feature is the spatial extent of the glints. Many of the more intense features are spatially resolved with angular extents of 0.2 to 0.8 mrad. Similarly, inspection of the sequential scans (a) through (d) in Figure 9, each separated in time by 0.1 second, indicates that the more intense glints often have durations of 0.1, 0.2, or even 0.3 seconds.

A spectral comparison of one scan of the observed sun glint scene is shown in Figure 10. No spatial correlation is expected or observed between the various spectral bands because of the quickly varying nature of the scene and the $\sim$10 second time interval between scans of the separate spectral bands. The intensity variations between the spectral bands are striking. Here, as in the cloud measurement, the red spike (4.4 - 4.8 μm) spectral band shows the smallest radiance variations. In contrast to the cloud data, however, the blue spike band (3.8 - 4.2 μm) is also much quieter than the two wide passbands.

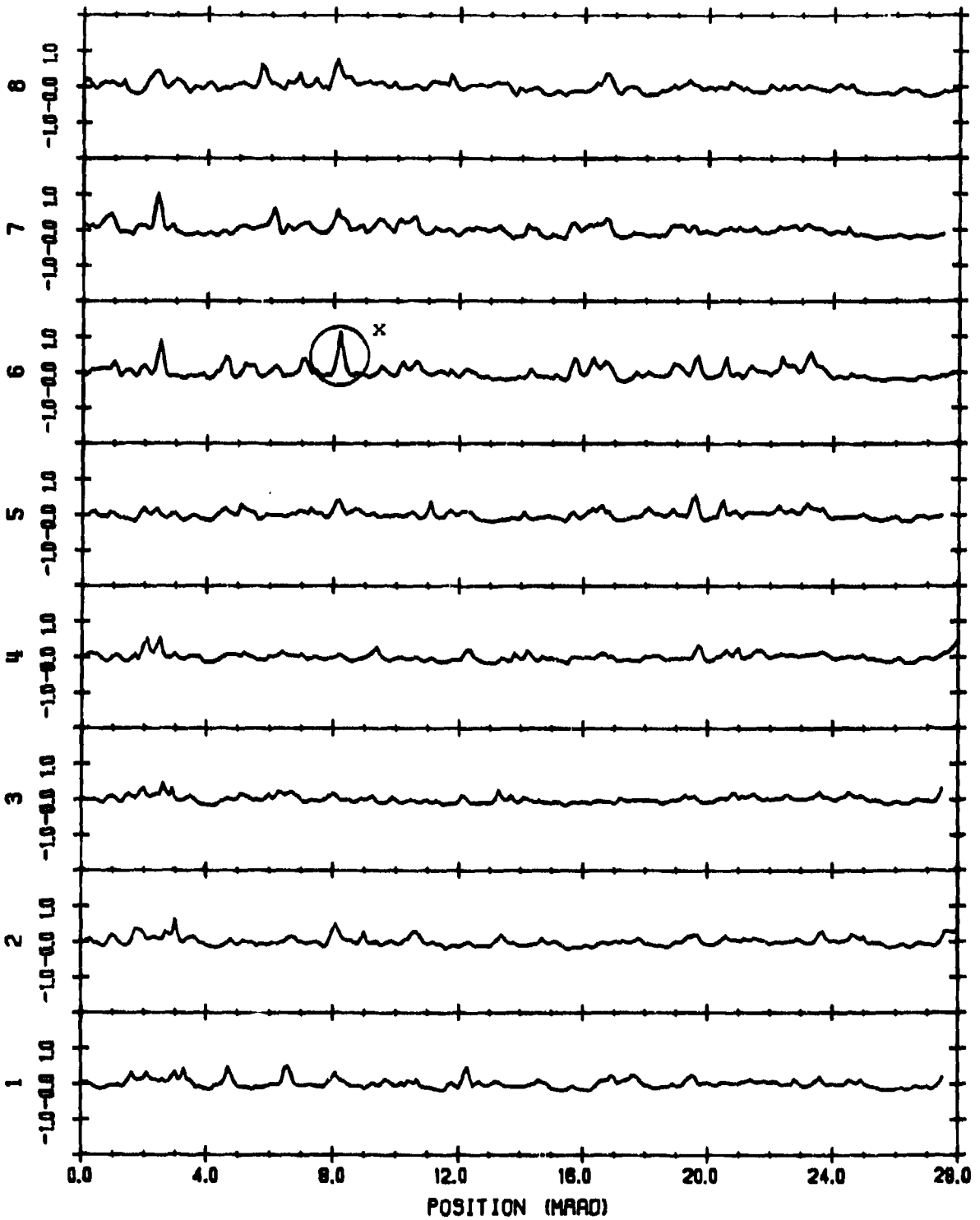

Fig. 9(a) – Radiant exitance (10^{-3} w/cm^2) presented as a function of channel number for scene #5 (ocean sunglint) Scan #1, Filter #1. (Note circled glint labeled "x" persists on the following figures indicating a duration of about 0.3 second).

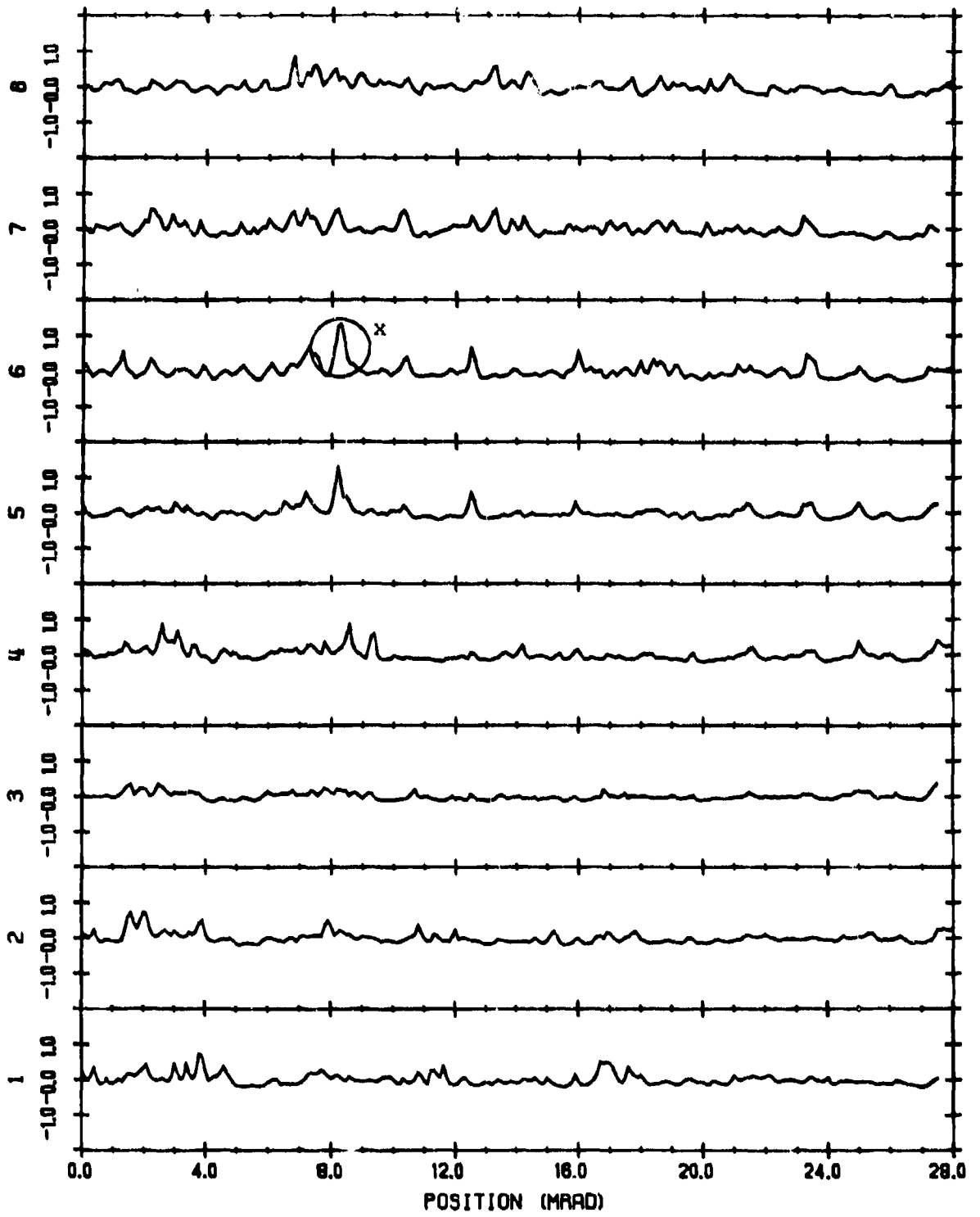

Fig. 9(b) — Radiant exitance (10^{-3} w/cm^2) presented as a function of channel number for scene #5 (ocean sunglint), Scan #2, Filter #1.

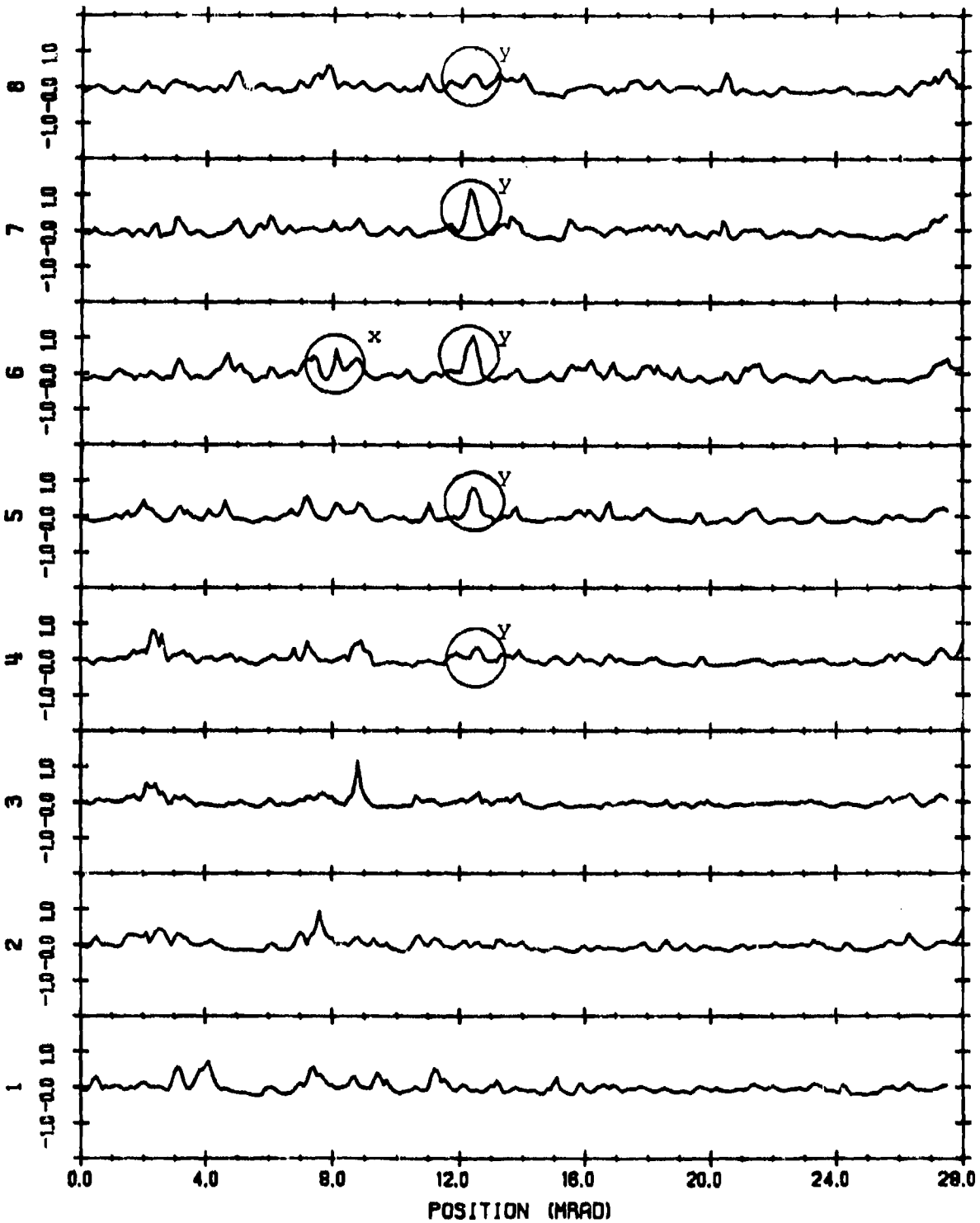

Fig. 9(c) — Radiant exitance (10^{-3} w/cm^2) presented as a function of channel number for scene #5, (ocean sunglint) Scan #3, Filter #1. (Note circled glint labeled "y" indicates a glint width of about 0.4 milliradian.)

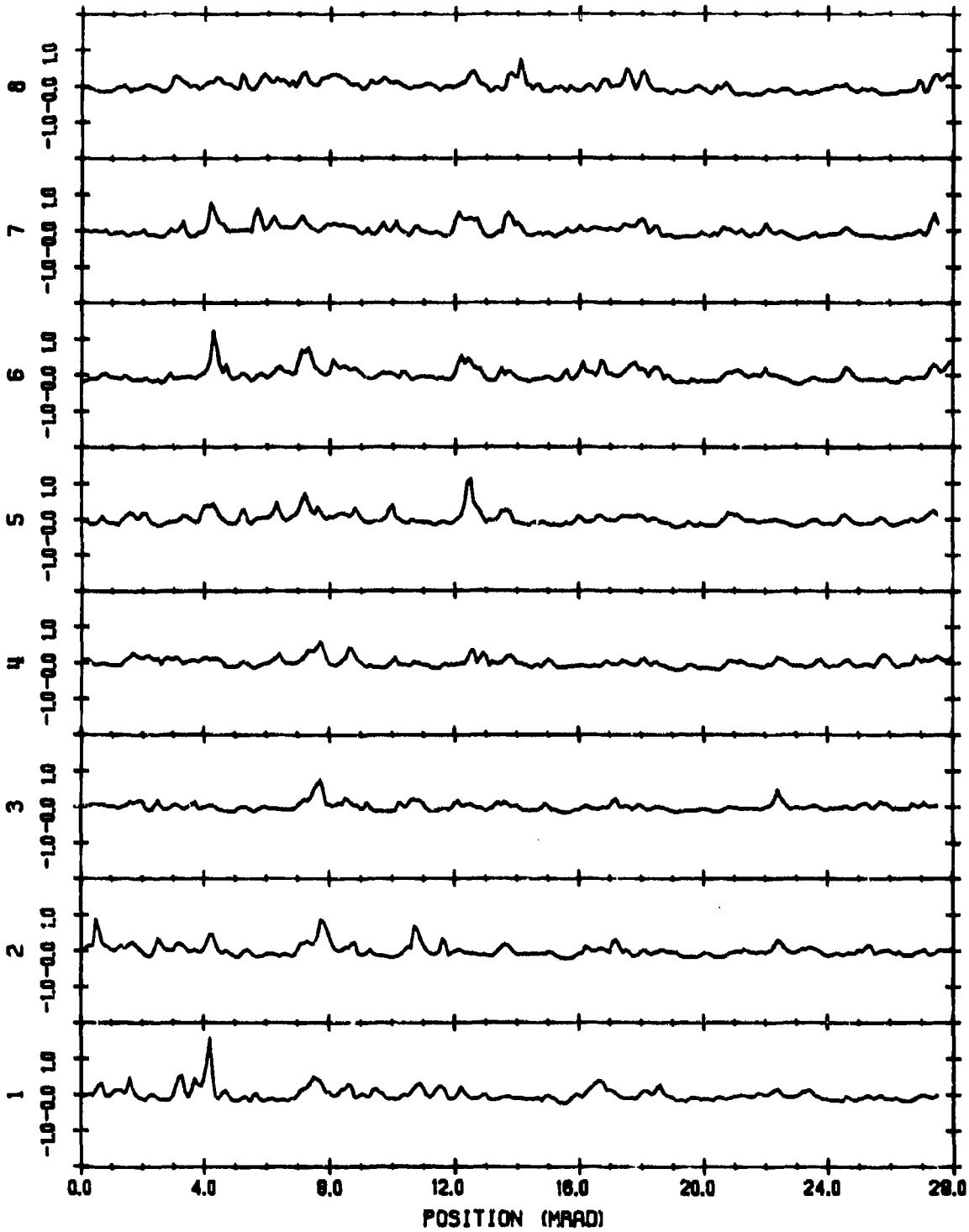

Fig. 9(d) — Radiant exitance (10^{-3} w/cm^2) presented as a function of channel number for scene #5 (ocean sunglint), Scan #4, Filter #1.

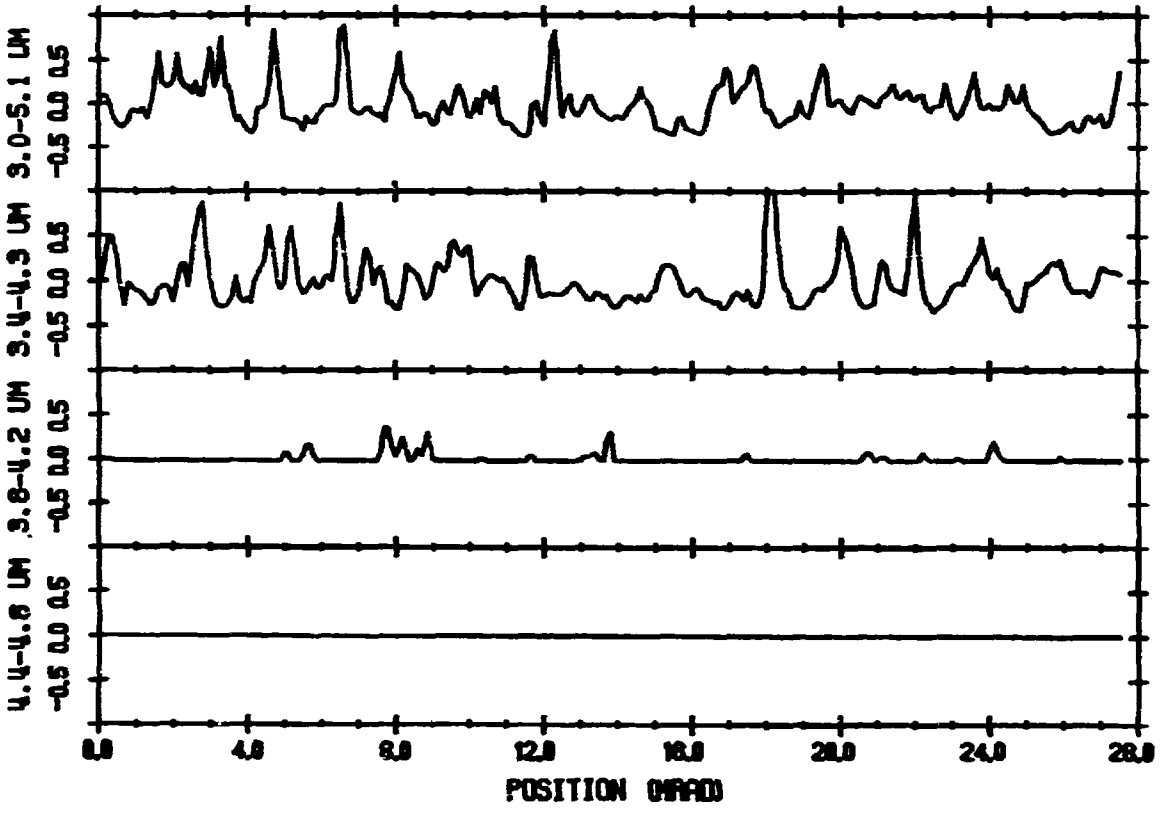

Fig. 10 — Radiant exitance (10^{-3} w/cm^2) presented as a function of spectral bandpass for scene #5 (ocean sunglint), Scan #1, Channel #1).

6
SUMMARY AND RECOMMENDATIONS

6.1 SUMMARY

A digital tape has been prepared including eight cloud background scenes and one ocean sun glitter scene as measured with a high sensitivity scanning radiometric system. Analyses of these data have indicated that the results are reasonable and should prove valuable in future work. Steps have been outlined to improve measurement and data reduction procedures. The accuracy of the current data is summarized in Table 6. Despite some of the limitations of the data, they probably represent the best set of such background data currently available.

6.2 RECOMMENDATIONS FOR FUTURE PROCEDURES

During the course of the study a number of potential improvements were identified in the CECO data acquisition procedures, and in the OptiMetrics data reduction procedures, which would improve the quality of the data obtained in future programs. Some of these recommendations for future improvements are summarized in Table 7.

We further note that the MIDAS III system had 24 detectors sensitive in the 3 - 5 μm, although signals from only eight of these were recorded. We recommend that data from the full array be recorded in future measurements. This would allow quantification of the degradation in cross-channel correlation as the elevation IFOV is increased. This would in turn allow a better assessment of the spatial resolution required for background suppression in IRST designs.

As is apparent from Table 6, tape recorder noise is the dominant noise type in the present data set. Toward eliminating this problem in future IR backgrounds measurements we suggest maintaining a minimum signal-to-noise ratio of 10 (recorded signal to rms tape noise).

TABLE 6. SUMMARY OF DATA COLLECTION AND REDUCTION UNCERTAINTIES. RADIANT EXITANCE VALUES ARE SHOWN FOR SPECTRAL FILTER #1

SOURCE OF ERROR	MAGNITUDE (VOLTS)	EQUIVALENT RADIANT EXITANCE (w/cm^2)
DETECTOR NOISE		$\pm 6 \times 10^{-6}$
TAPE RECORDER NOISE*	$\pm$ .018	$\pm 3 \times 10^{-5}$
A-D CONVERTER NOISE	$\pm$ .020	$\pm 3 \times 10^{-6}$
DC DRIFT UNCERTAINTY	REFER TO SECTION 3.2	
ELECTRONIC CALIBRATION UNCERTAINTY	REFER TO SECTION 3.2	

* Inspection of the CECO data suggests that the value $\pm 1 \times 10^{-5}$ w/cm^2 is a more realistic estimate for the signal-dependent tape noise than the nominal value quoted in the table.

Additional recommendations are described below, concerning:

- DC restoration
- Coordination with other measurement activities
- Selectivity in reducing additional Key West data
- Recommendations for future analysis

6.3 DC RESTORATION

We recommend that the MIDAS III sensor be upgraded to incorporate internal sources for DC restoration. Once

TABLE 7. RECOMMENDATIONS FOR IMPROVED BACKGROUND DATA ACQUISITION AND REDUCTION PROCEDURES

RECOMMENDATIONS	RESULTS
DATA ACQUISITION	
Correct tape speed malfunction	Elimination of drift in DC level
Record frequent electronic and radiance calibrations	Higher accuracy and confidence in calibration factors
Increase gain of weak signals before input to tape recorder	Moves weak signal out of tape and digitization noise
Record low frequency square wave calibration	Easier calibration signal to use than current 1 KHz sine wave
Simultaneously record sync signal on an odd and even tape channel	Allows more accurate data alignment when data are reduced on another analog tape recorder
Change spectral filter wheel more rapidly	Facilitates spectral comparison
Provide carefully boresighted visual photos of each IR scene	Allows IR/visual comparisons
Record IRIG time on all data tapes	Easier to correct interchannel spatial realignments and perform other data manipulations
DATA REDUCTION	
Perform simultaneous digitization of all channels	Better alignment of channel to channel data
Perform digitization with a higher A/D resolution	Better accuracy

DC-restored background signatures are available, we should be able to address such questions as: To what degree are target and background signatures coupled? Under what conditions and by what analytical procedures can target signatures be implanted into separately-measured background signatures?

DC restoration is a key element in integrating the existing data base of target signatures with any future data base of background signatures.

6.4 COORDINATION WITH OTHER MEASUREMENT ACTIVITIES

Background measurement sensors such as the CECO MIDAS radiometer can rapidly record far more data than can be economically reduced and analyzed. Thus, it is desirable to pre-screen the unreduced data in some fashion to eliminate what would subsequently prove to be relatively benign and uninteresting data.

In the present instance, the data were pre-screened by two of the authors (R. Steinberg and F. Smith) who visually inspected the video oscillographs, and selected for analysis those scenes that displayed relatively large amplitude and fine-scale structure.

In principle, a better way to assure the collection of interesting data is to co-locate the background measuring equipment with an IR surveillance sensor (IRSS). Each false alarm experienced by the IRSS can be used to direct the background sensor's line of sight toward a significant structural feature in the IR scene.

Preliminary steps along these lines were made at Key West, the CECO radiometer having been co-located with an IRSS. In fact, our interest in reducing Scene

42 (Fig. 8) was motivated by the IRSS having declared the presence of a clutter in this scene.

Inspection of Fig. 8 shows that our Scene 42 data is mainly tape noise. Thus, CECO's attempt to quantify the structure of the IRSS clutter artifact was not successful. A possible explanation is that the two sensors were not adequately boresighted, i.e., that coordination between the two measurement activities was insufficient to achieve the desired objective of quickly and reliably focusing the MIDAS field-of-view on artifacts cued by the IR surveillance device.

There is, however, a second possible explanation for the apparent absence of a clutter artifact in Fig. 8. If the noise equivalent exitance of the IRSS is less than that of the CECO radiometer/tape recorder, scene 42 may indeed contain an important artifact whose presence in Fig. 8 is obscured by tape recorder noise. This type of ambiguity in data interpretation can only be eliminated by making sure that the background sensor (including tape recorder) has a lower noise equivalent exitance than the co-located IRSS.

6.5 SELECTIVITY IN REDUCING ADDITIONAL KEY WEST DATA

The digital data tape documented in this report contains only 9 of the original 58 scenes for which CECO has obtained analog background video. These nine scenes were chosen by visually inspecting video oscillographs for all 58 scenes, and selecting only those scenes that displayed relatively large amplitudes and large gradients (except for scenes 31 and 42, which were selected by different criteria).

Most of the scenes which were not selected displayed little structure. (See the video oscillographs in the Appendix of Reference 1.) Thus, wholesale reduction of the remaining 49 scenes is not recommended at this time. However, analysis of the reduced data described in this report may suggest the need to reduce additional selected elements of the 49 unreduced scenes.

6.6 RECOMMENDATIONS FOR FUTURE ANALYSIS

The present study has only briefly analyzed the reduced data presented here. Further analysis of the data is desirable in three areas:

- Comparisons with and development of physical models,
- Analysis of statistical characteristics of the scenes, and
- Development and evaluation of background discrimination algorithms using the data.

In the area of physical modeling, the data could be used to check the predictions of single and multiple scattering radiance models against the measured results.

Semi-empirical models could be developed and evaluated using such simple approaches as the diffusely reflecting cloud model described in Section 5. One important aspect which could be investigated is the spatial gradients in the cloud-edge regions for the various spectral bands.

A number of statistical questions arise from inspection of the data. Such simple measures as means, standard deviations and histograms of the cloud scenes may be useful in characterizing the results. Temporal and spatial correlation functions may also be useful.

Although statistical measures may yield insight into the background data and even help guide the development of some clutter suppression techniques, background statistics are generally inadequate for system performance evaluation. In general, performance assessments of particular signal processing approaches appear to necessitate their simulation against the data base of background imagery [4].

REFERENCES

1. A. Geiser, C. Dippel, V. O'Connell and S. Bertke, Radiometric Measurements by the MIDAS III System at Key West, Volume 1: Cloud Backgrounds, Cincinnati Electronics Corp., CTR-79-0012, 19 September 1979.

2. G. Lindquist and R. Maxwell., Unpublished report on Warning Receiver Modeling, Environmental Research Institute of Michigan, Ann Arbor, MI.

3. G.W. Ashley, et al., "Background Spectral Radiance and Contrast in the Near-UV, Mid-IR, and LWIR Regions," TM6-125 PH-438, General Dynamics, Pomona Division, July 1975.

4. L.N. Peckham, F.A. Horrigan, L.L. Doran, and R.A. Steinberg, "Infrared Search and Track System Evaluation Model (IRSTEM)," EOTPO Report No. 59, Electro-Optical Technology Program Office, Naval Research Laboratory, Washington, D.C.

ACKNOWLEDGMENTS

The infrared background signatures described in this report were obtained by the Advanced Systems, Engineering Analysis, and Measurements Group of Cincinnati Electronics Co. (CECO), supervised by Louis Williams. The CECO project engineer was Al Geiser. Support for the CECO measurements was provided by Jon Wunderlich,Program Manager, Navy Optical Signatures Program. Support for reducing the data was provided by A. Fenner Milton, Head, EO Technology Branch, Naval Research Laboratory (NRL).

The CECO background measurements would not have been performed but for the interest and support of John M. MacCallum, Jr., Head, EO Technology Program Office, NRL.

APPENDIX A
SYSTEM RELATIVE SPECTRAL RESPONSE CHARACTERISTICS

The system relative spectral response (radiometer plus filter) of the Cincinnati Electronics Corporation MIDAS III radiometer is given in Figures A.1 - A.4 for each of the 3 - 5 μm wavebands, as obtained from Geiser, et al. [1].

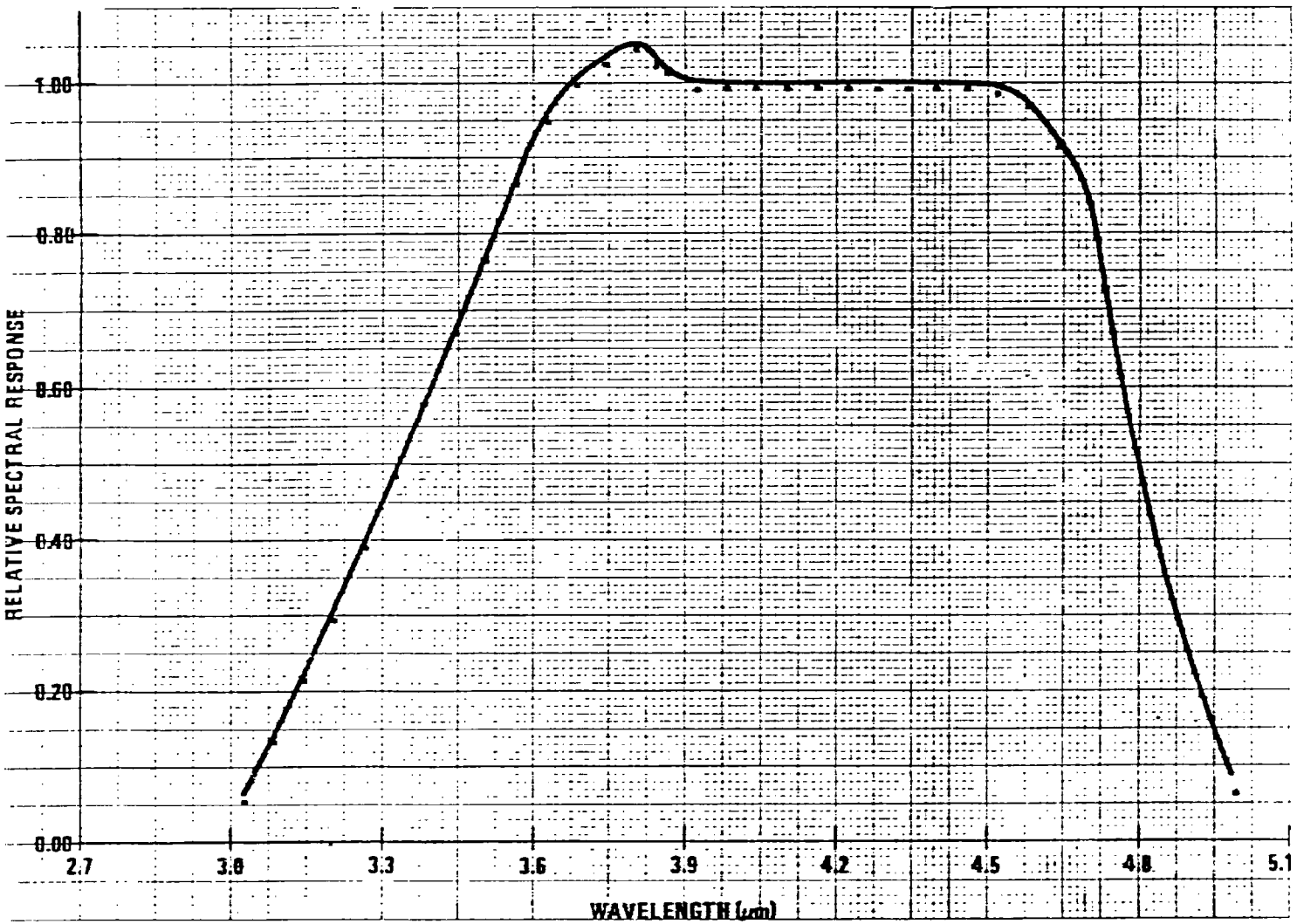

Fig. A.1 — System relative spectral response - Filter No. 1 (3.0 - 5.1 μm) (Obtained from Ref. 1).

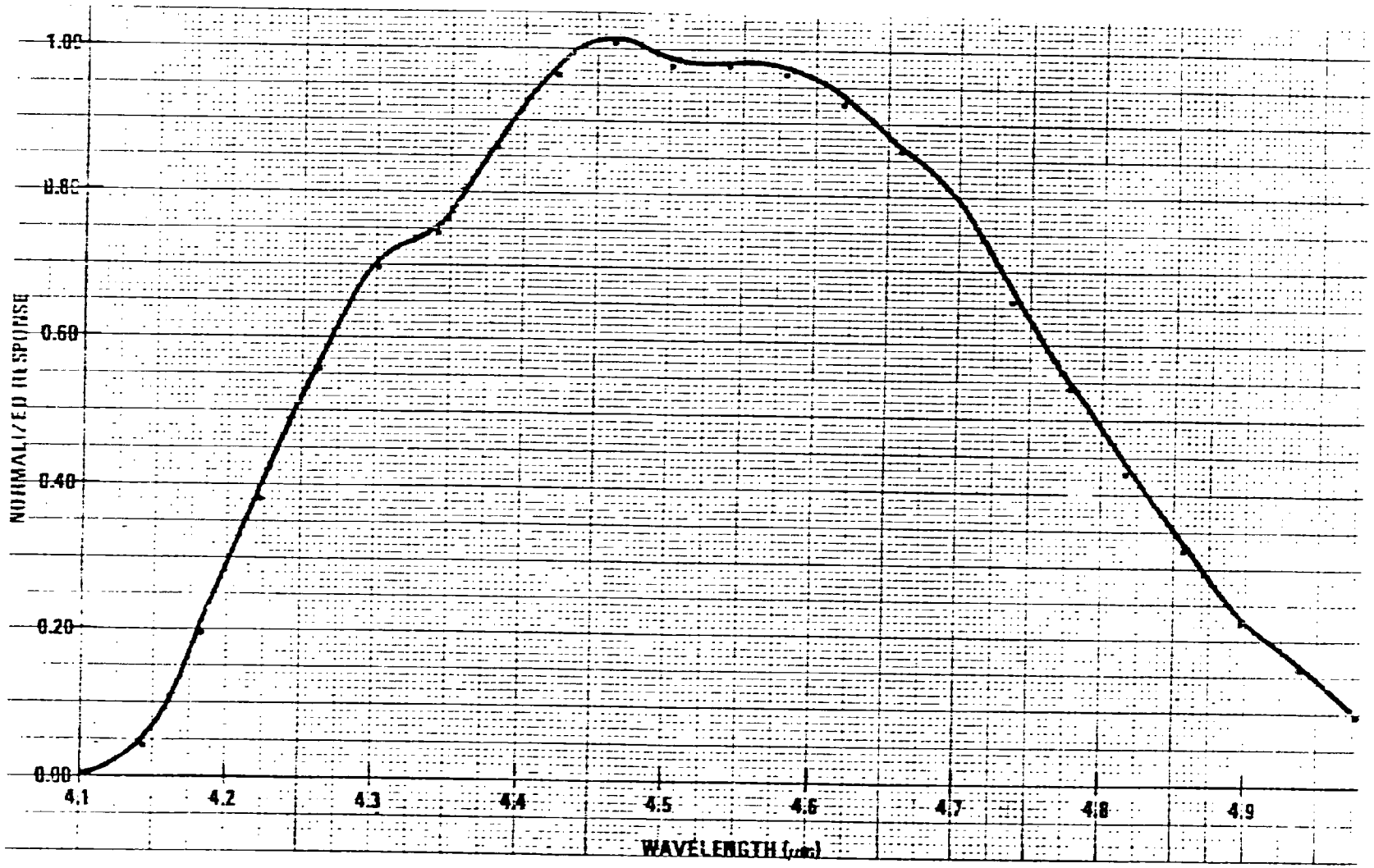

Fig. A.2 — System relative spectral response - Filter No. 2 (4.4 - 4.77 μm) (Obtained from Ref. 1).

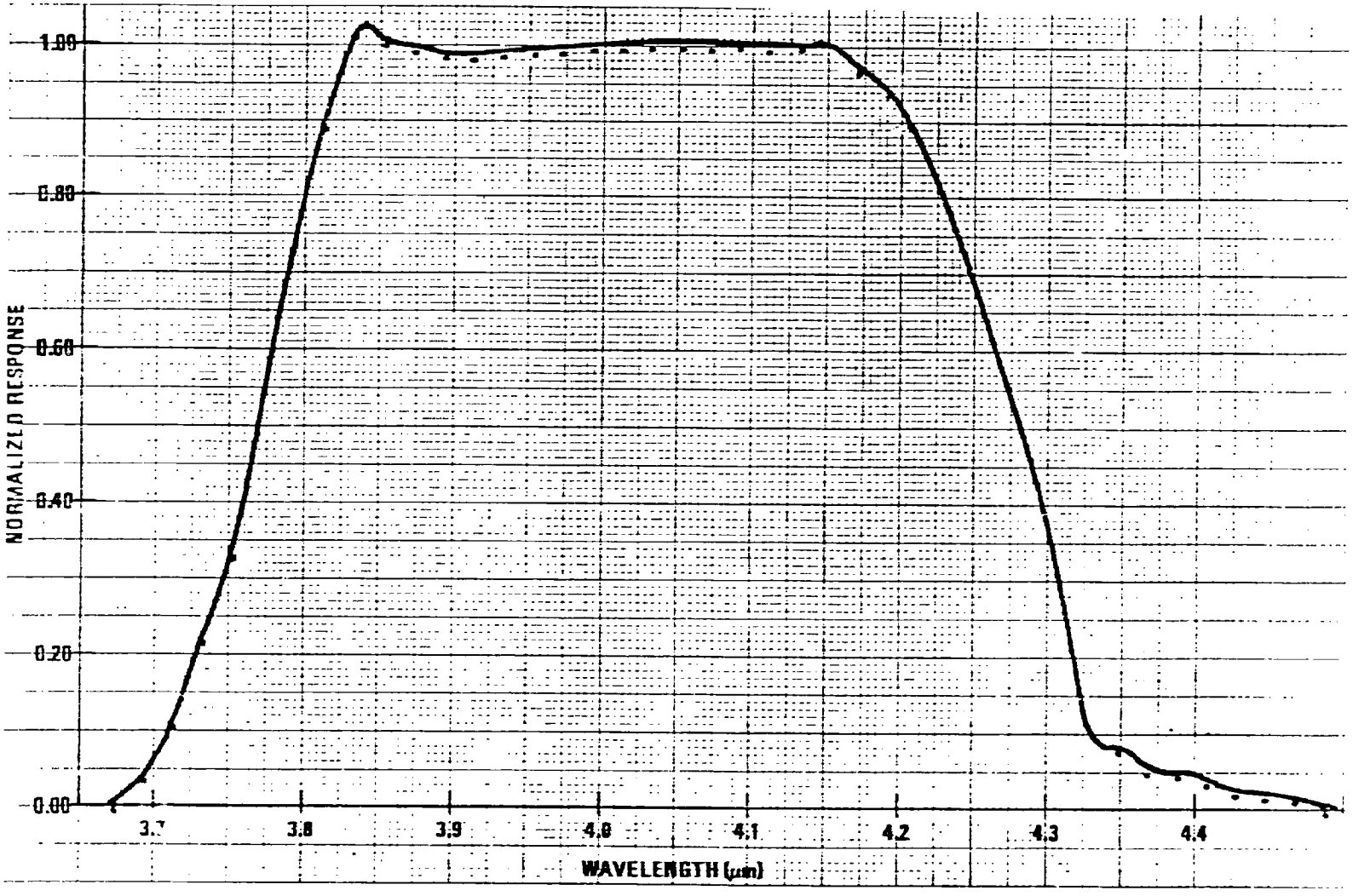

Fig. A.3 — System relative spectral response - Filter No. 5 (3.8 - 4.2 μm). (Obtained from Ref. 1.)

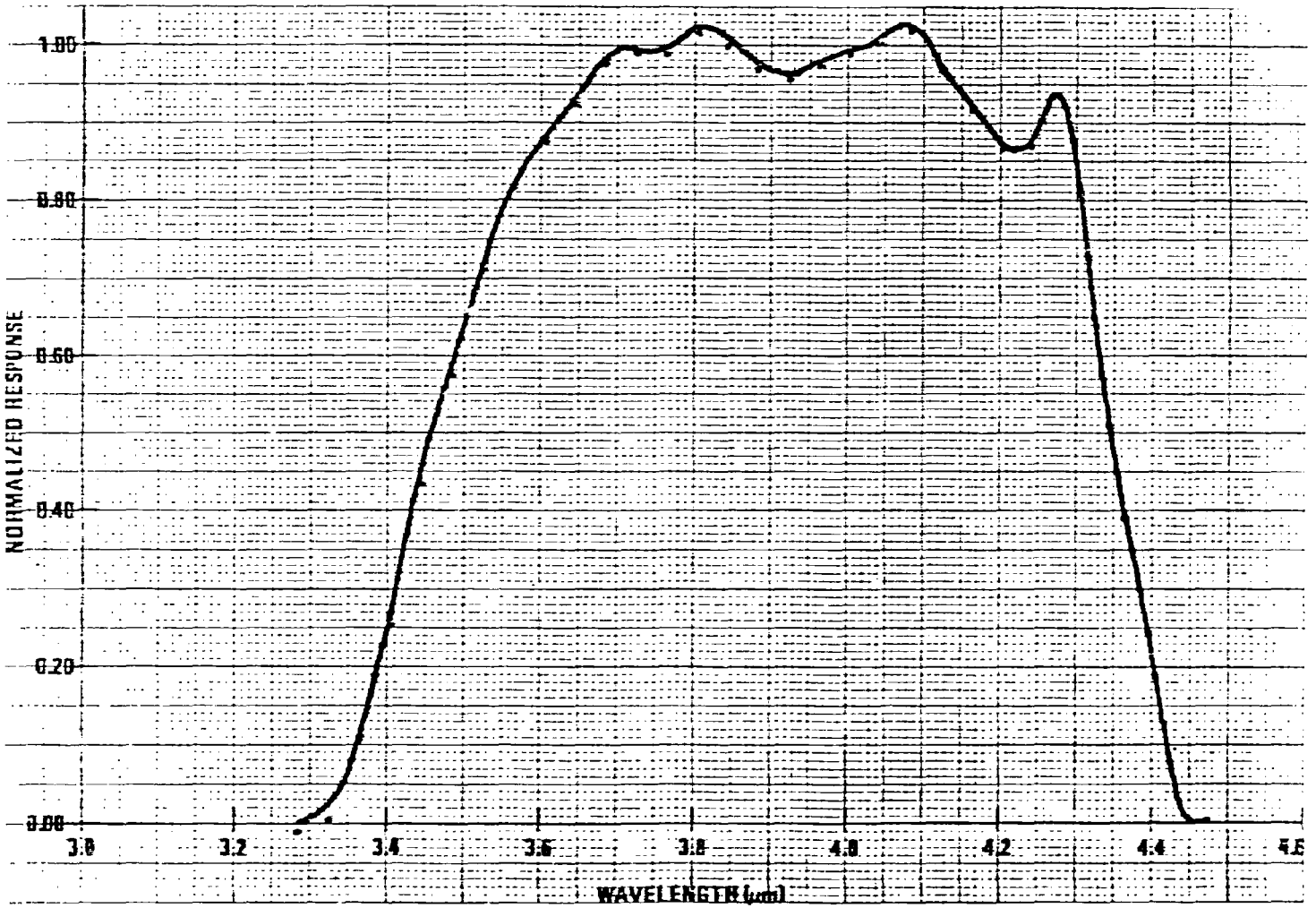

Fig. A.4 — System relative spectral response - Filter No. 6 (3.4 - 4.3 μm). (Obtained from Ref. 1).

APPENDIX B
SAMPLE DATA

The following sample data illustrate the results available for each digitized scene. Data from the various spectral regions are plotted on the same graph. However, note that the spectral scans are not simultaneous, differing by up to 60 seconds between scans. Also note that the intensity scale varies for the various scenes.

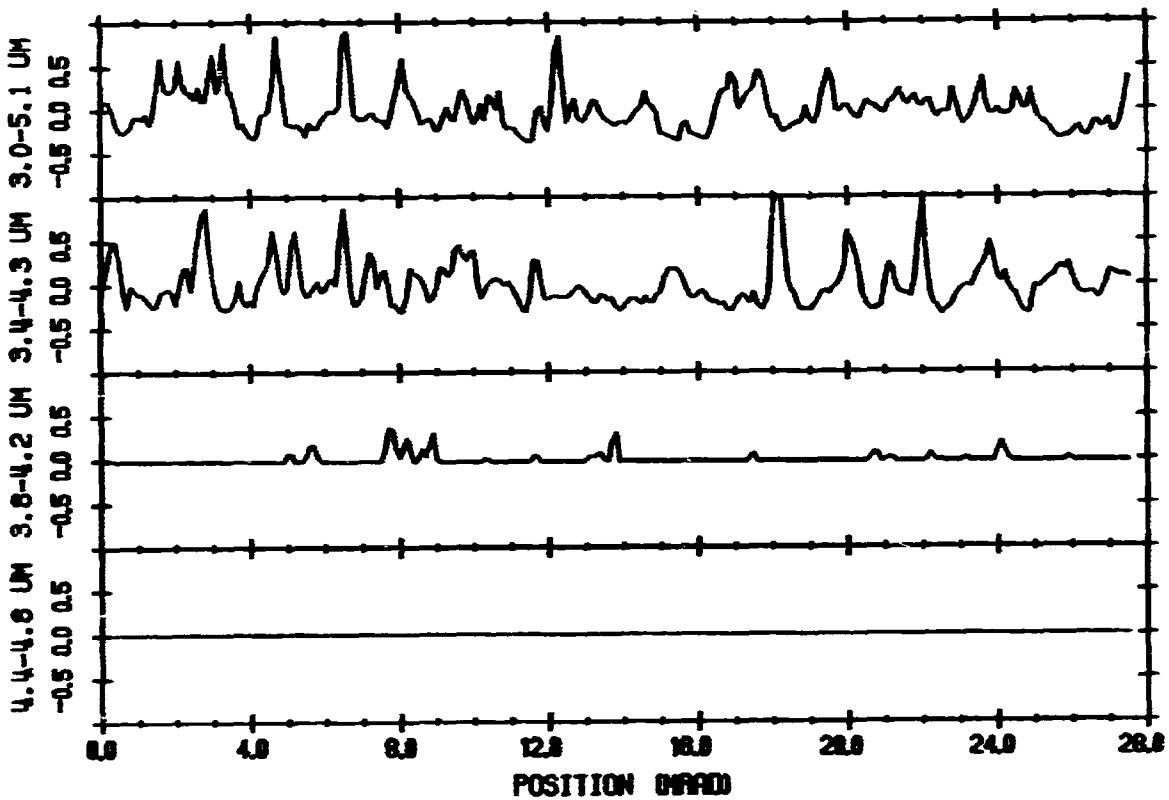

Fig. B.1 — Radiant exitance (10^{-3} w/cm^2) presented as a function of spectral bandpass for scene #5 (ocean sunglint), Scan #1, Channel #1.

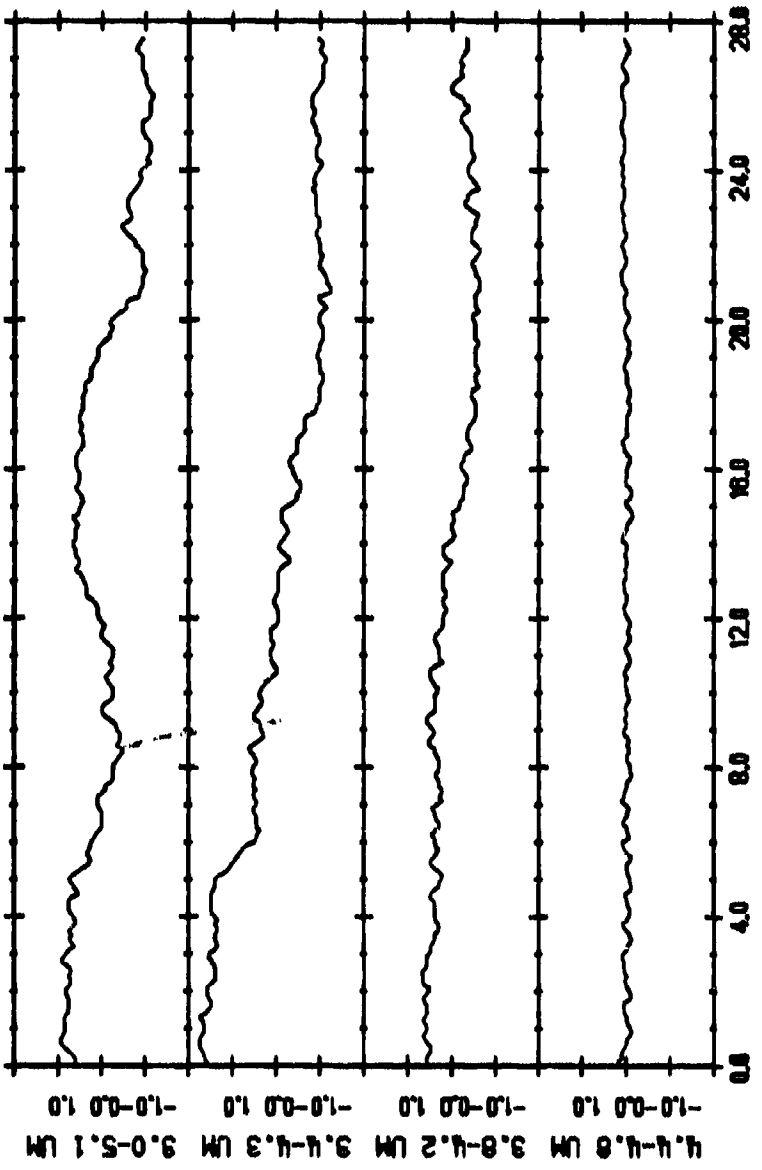

Fig. B.2 — Radiant exitance (10^{-4} w/cm^2) presented as a function of spectral bandpass for scene #8 (cloud), Scan #1, Channel #1.

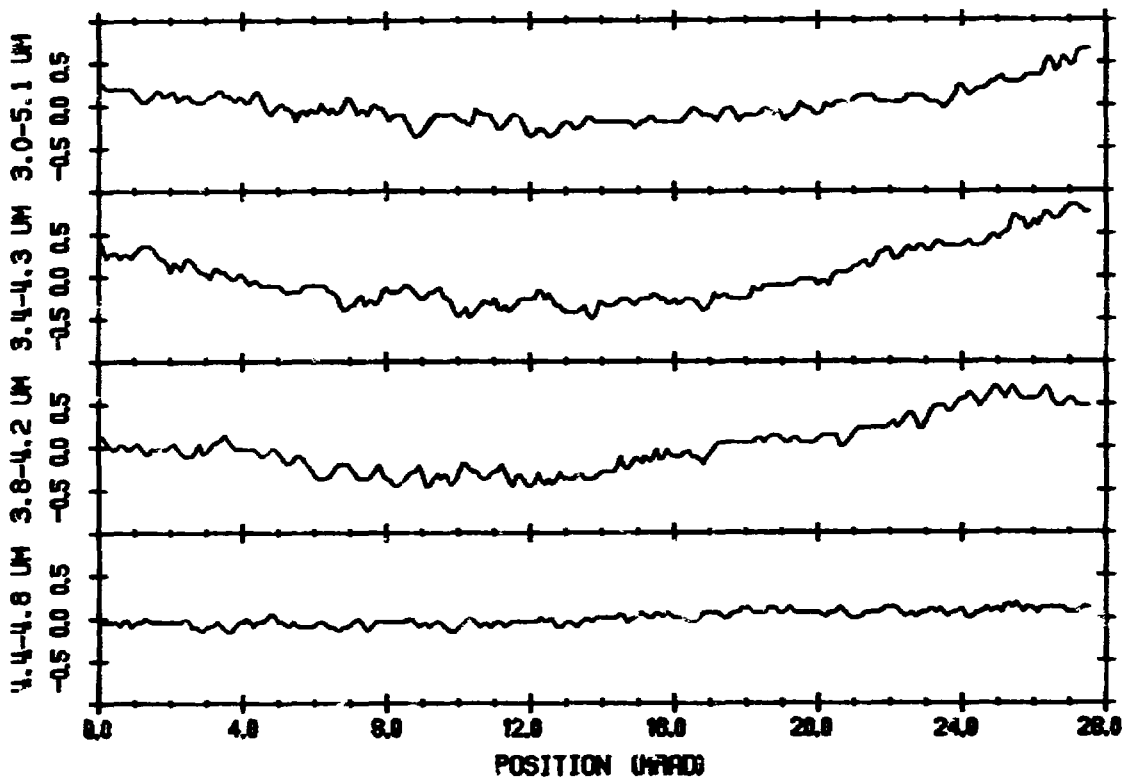

Fig. B.3 — Radiant exitance (10^{-4} w/cm^2) presented as a function of spectral bandpass for scene #11 (cloud), Scan #1, Channel #1.

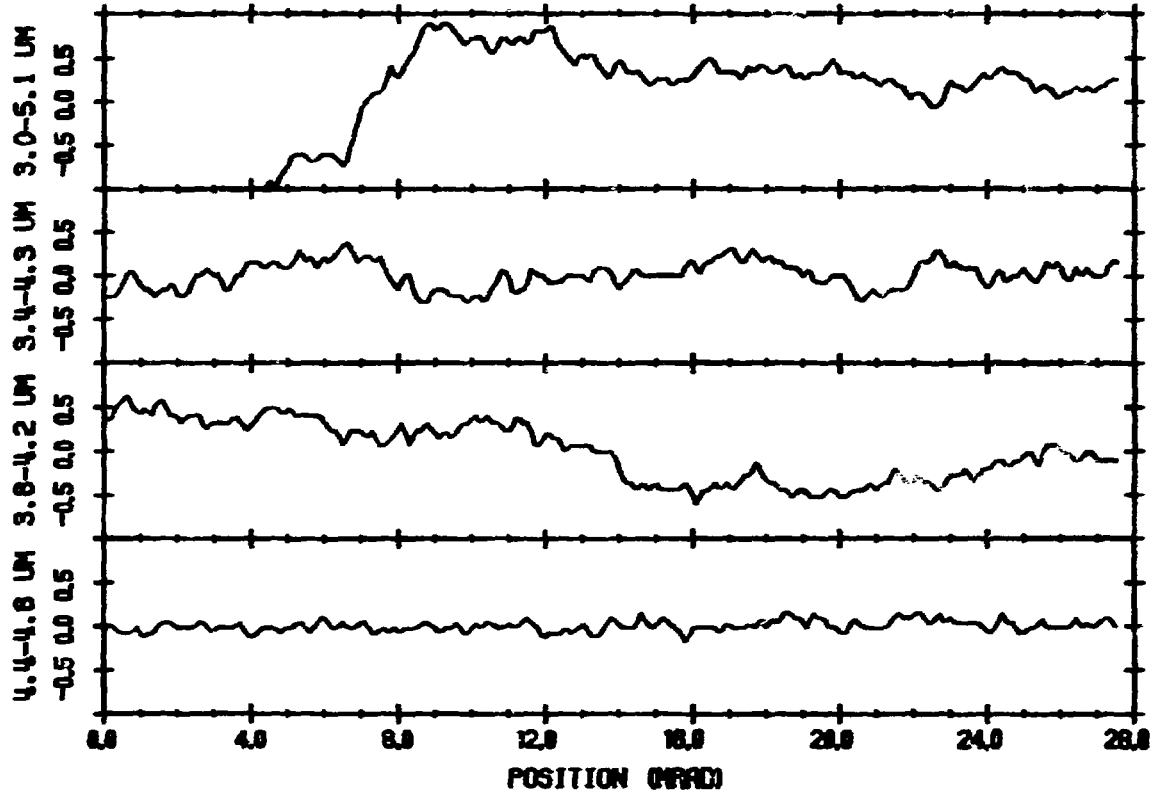

Fig. B.4 — Radiant exitance (10^{-4} w/cm^2) presented as a function of spectral bandpass for scene #18 (cloud), Scan #1, Channel #1.

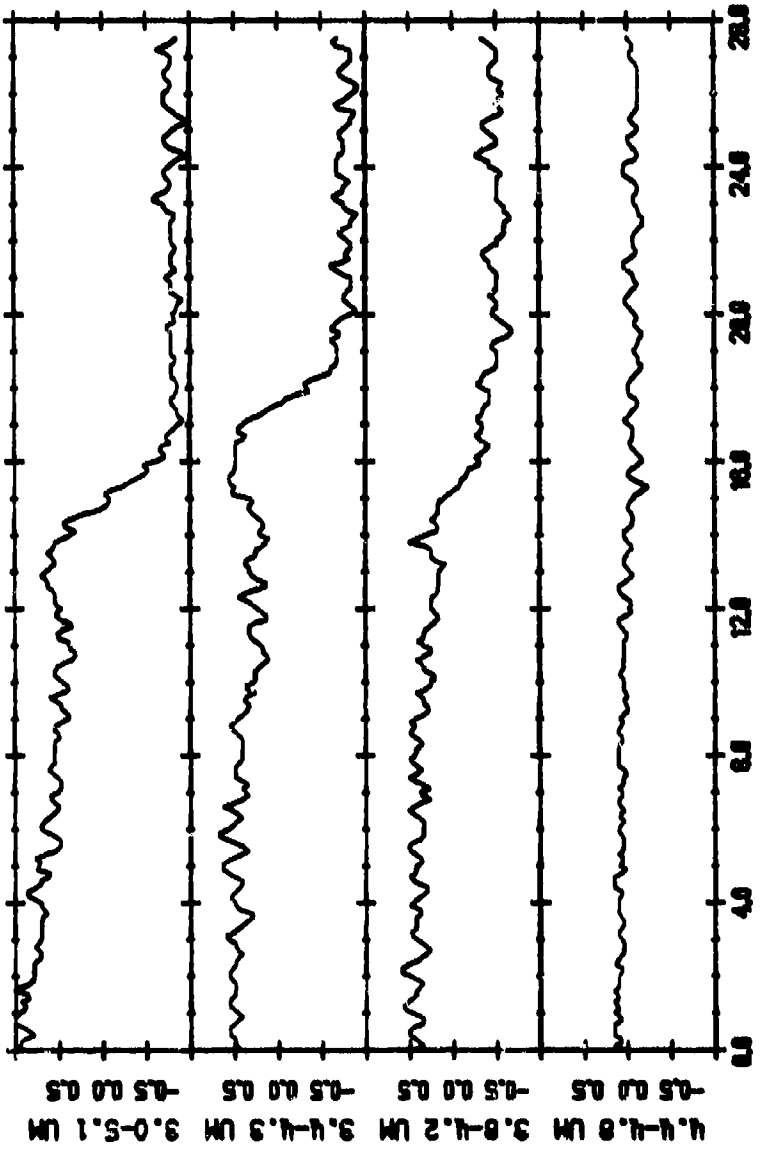

Fig. B.5 — Radiant exitance (10^{-4} w/cm^2) presented as a function of spectral bandpass for scene #28 (cloud), Scan #1, Channel #1.

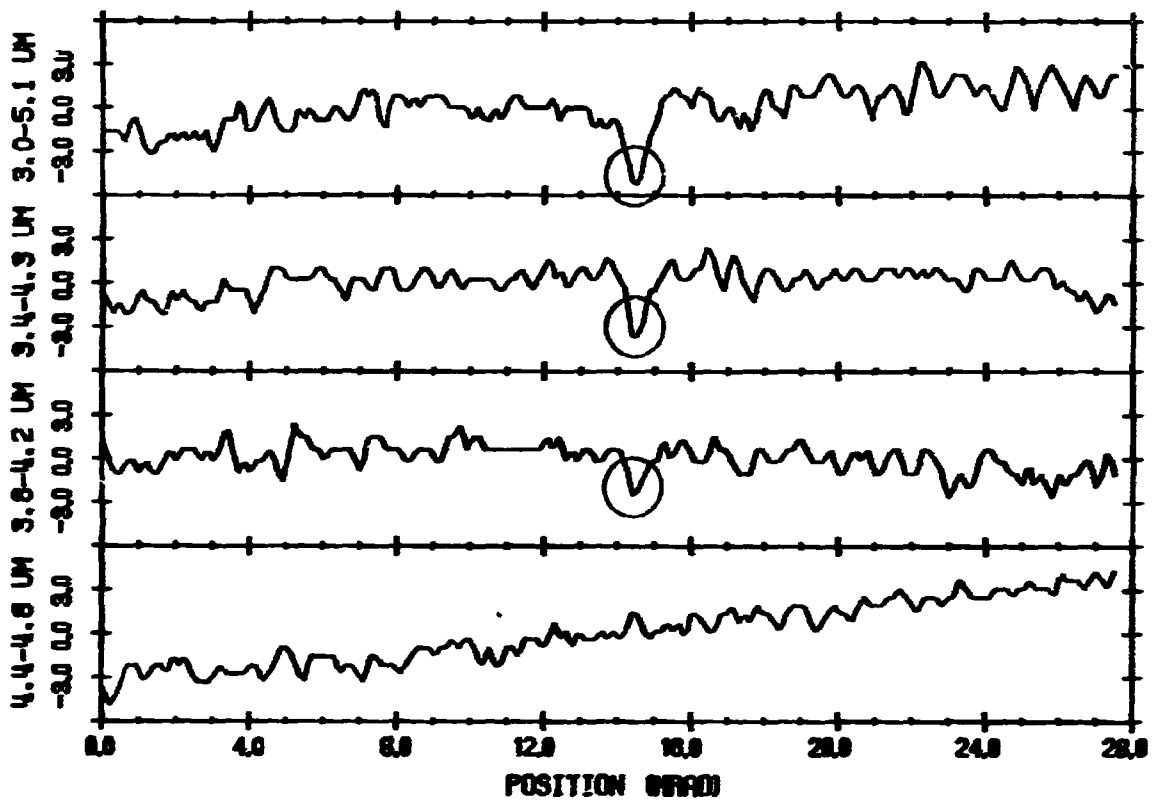

Fig. B.6 — Radiant exitance (10^{-5} w/cm^2) presented as a function of spectral bandpass for scene #31 (Microwave tower), Scan #1, Channel #1. Data are largely dominated by tape noise, except for tower (circled).

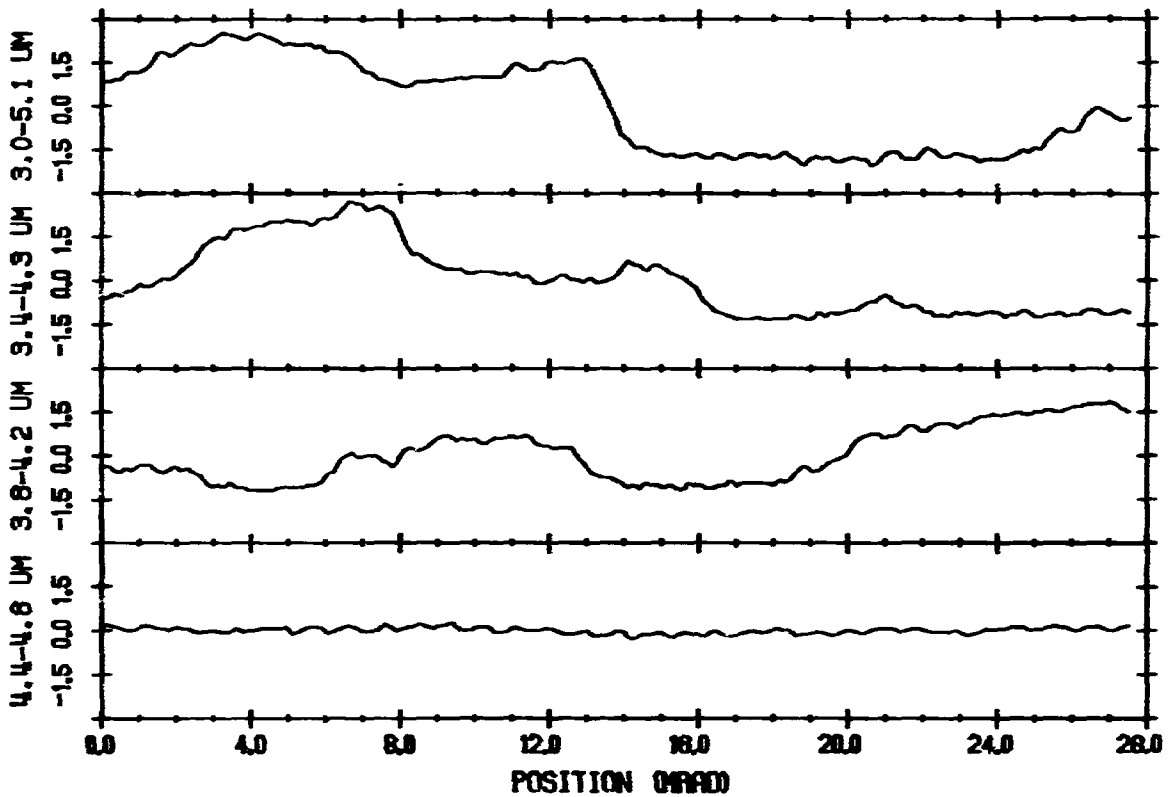

Fig. B.7 — Radiant exitance (10^{-4} w/cm^2) presented as a function of spectral bandpass for scene #35 (cloud), Scan #1, Channel #1.

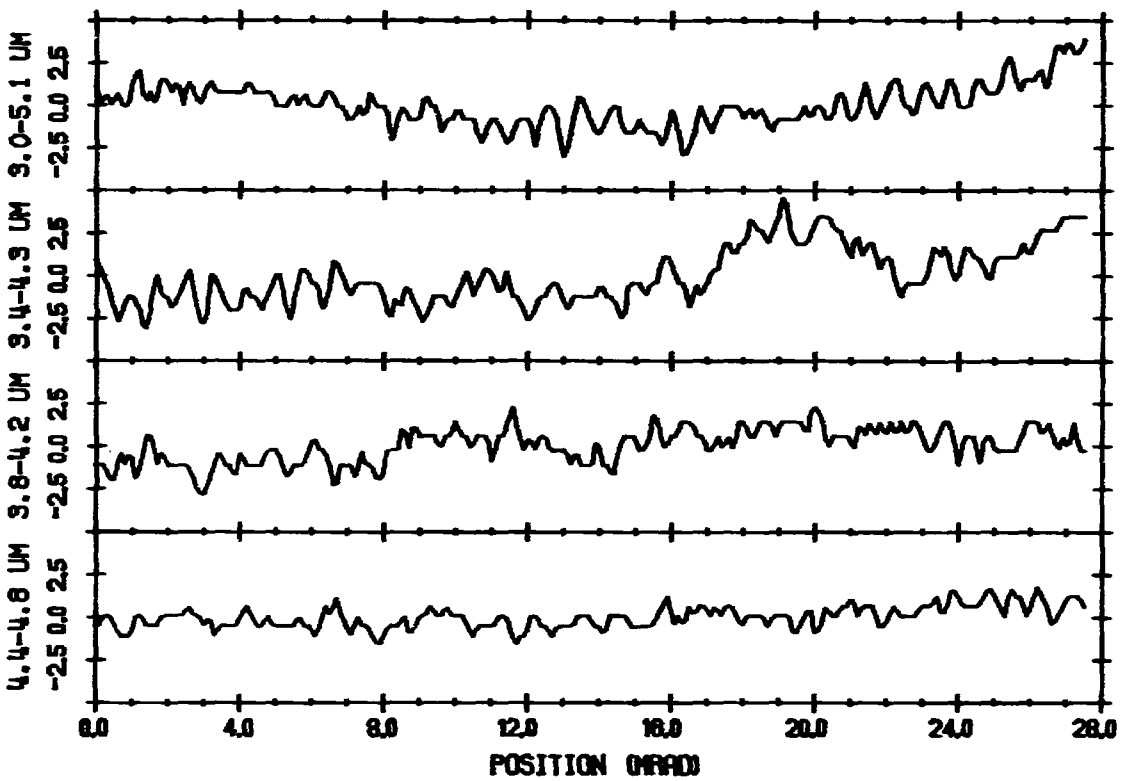

Fig. B.8 — Radiant exitance (10^{-5} w/cm^2) presented as a function of spectral bandpass for scene #42 (cloud deck near horizon), Scan #1, Channel #1. Data are largely dominated by tape noise.

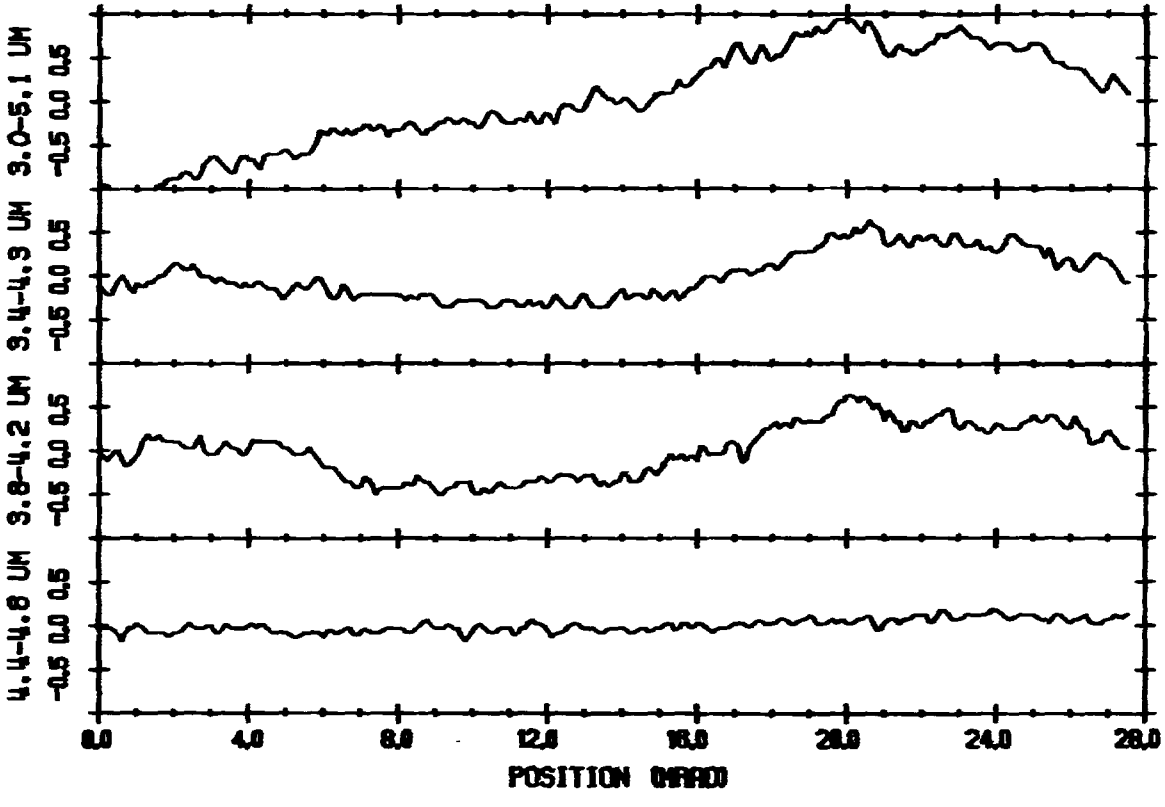

Fig. B.9 — Radiant exitance (10^{-4} w/cm^2) presented as a function of spectral bandpass for scene #57 (cloud), Scan #1, Channel #1.

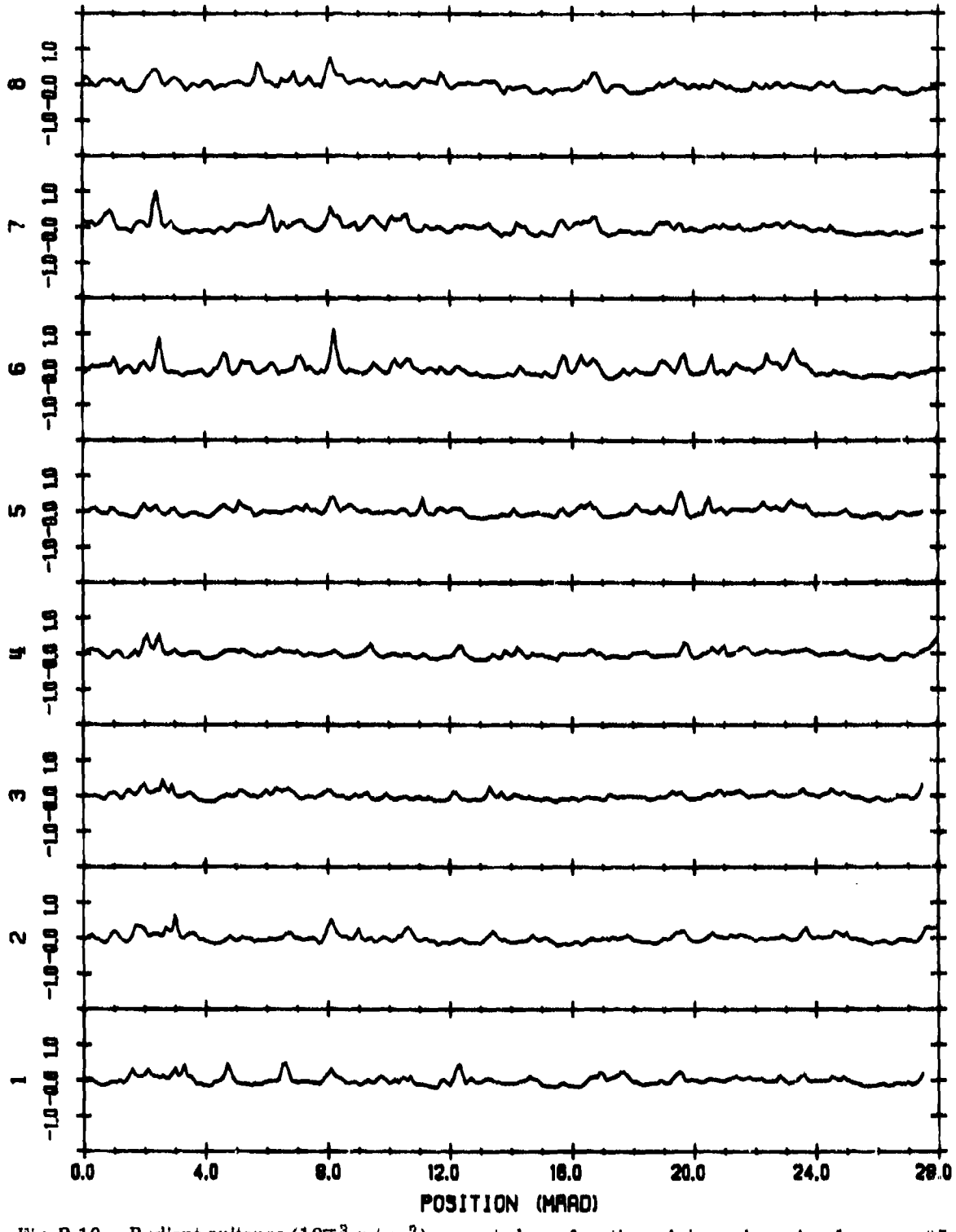

Fig. B.10 — Radiant exitance (10^{-3} w/cm^2) presented as a function of channel number for scene #5 (ocean sunglint), Scan #1, Filter #1.

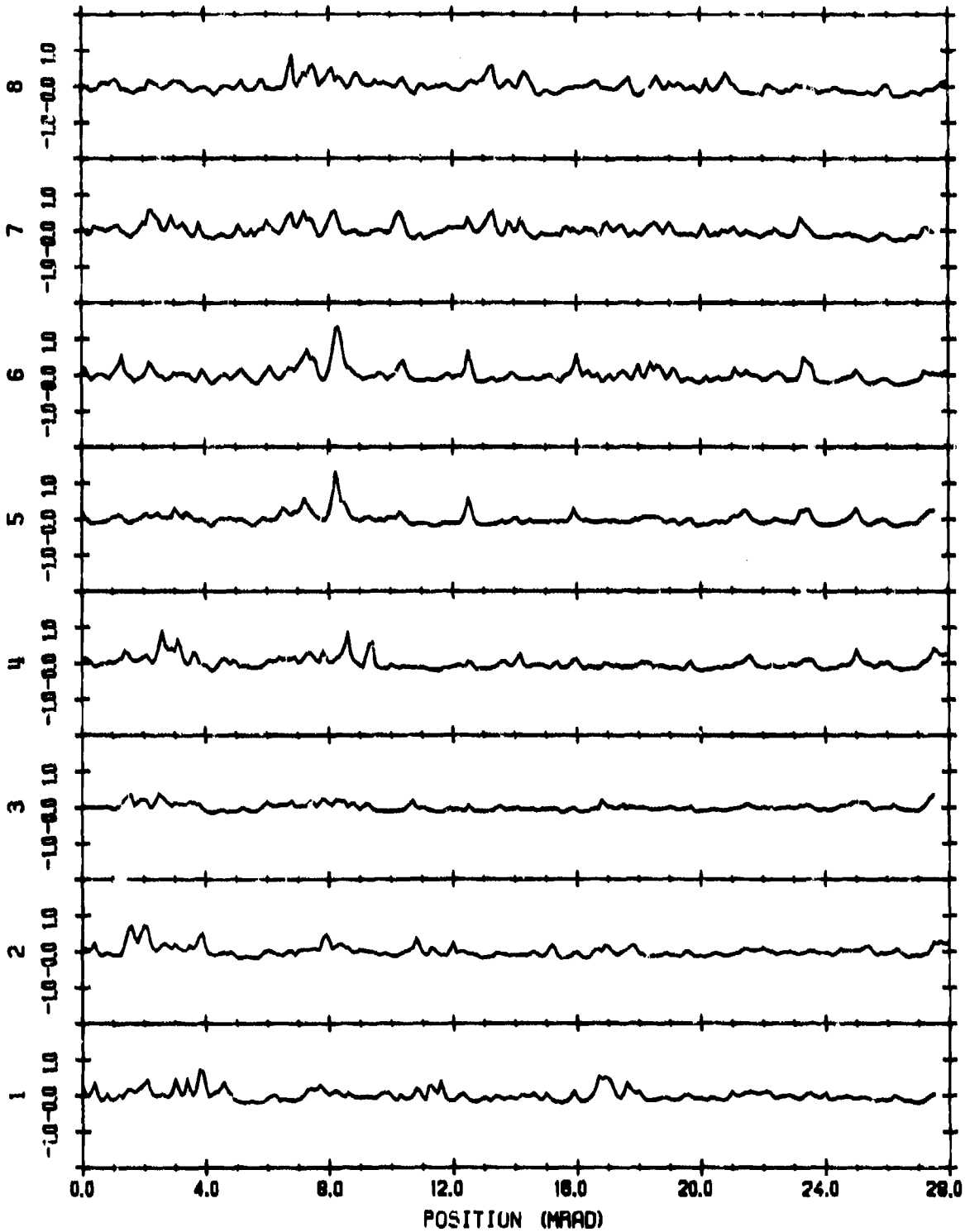

Fig. B.11 — Radiant exitance (10^{-2} w/cm^2) presented as a function of channel number for scene #5 (ocean sunglint), Scan #2, Filter #1.

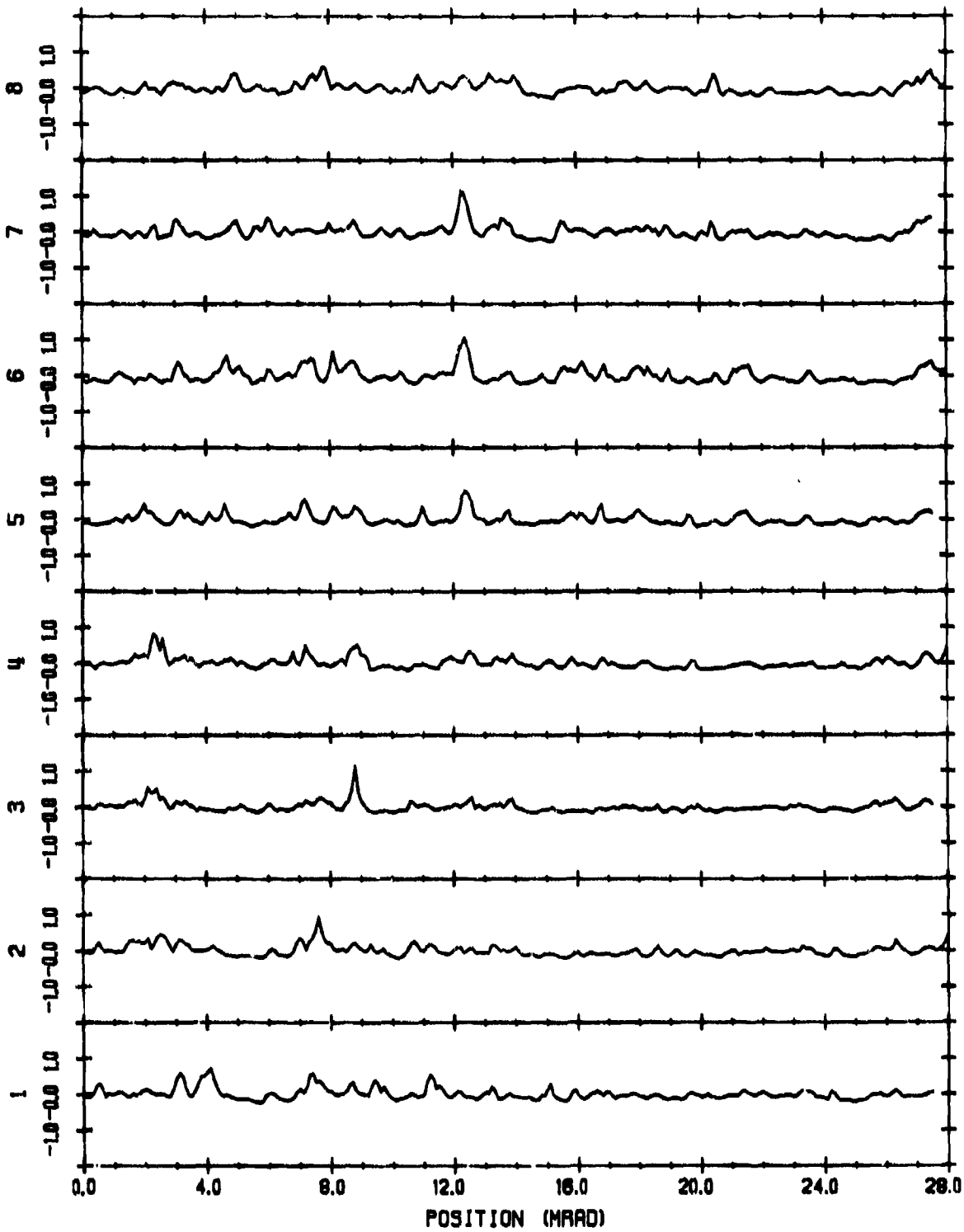

Fig. B.12 — Radiant exitance (10^{-3} w/cm^2) presented as a function of channel number for scene #5 (ocean sunglint), Scan #3, Filter #1.

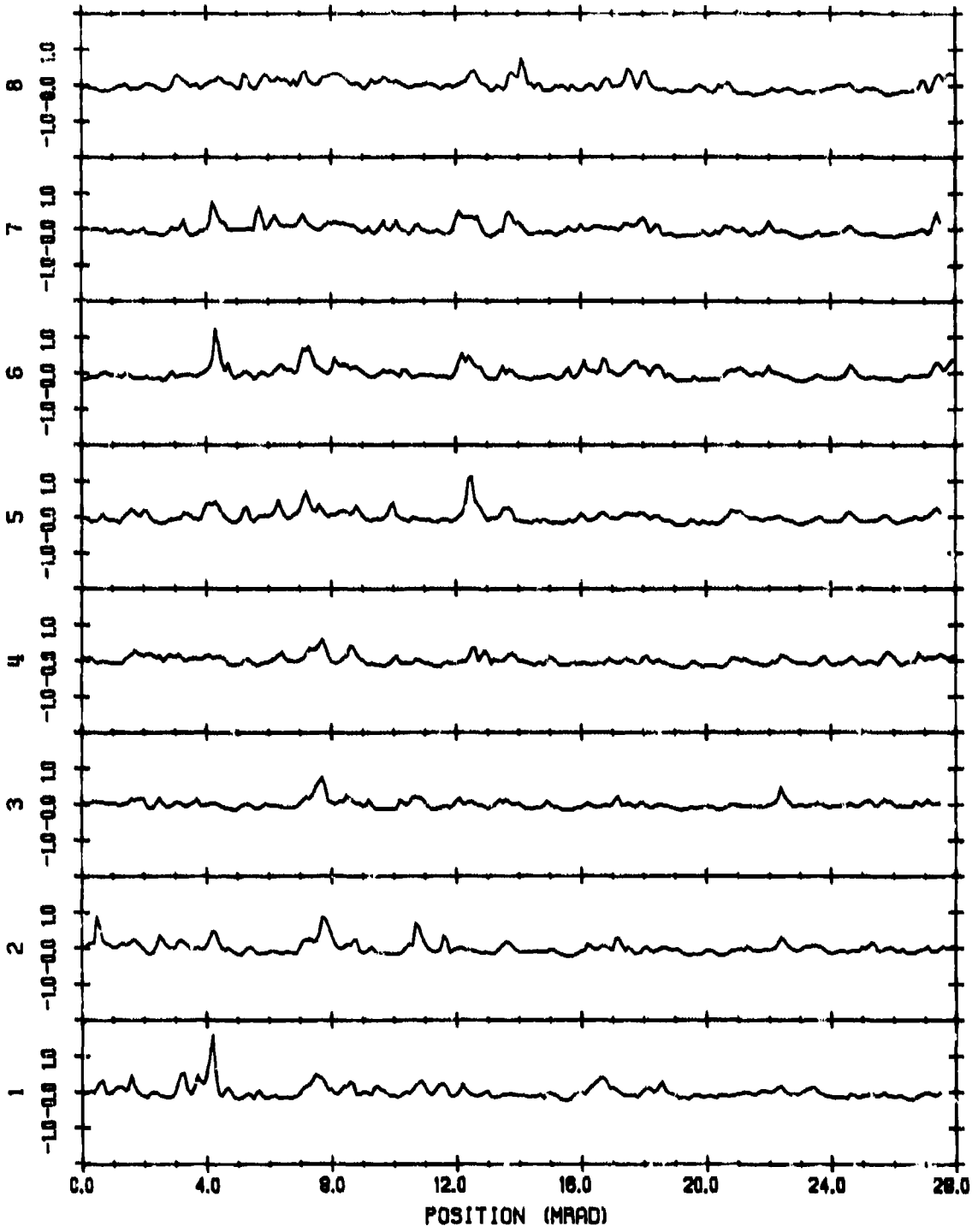

Fig. B.13 — Radiant exitance (10^{-3} w/cm^2) presented as a function of channel number for scene #5 (ocean sunglint), Scan #4, Filter # 1.

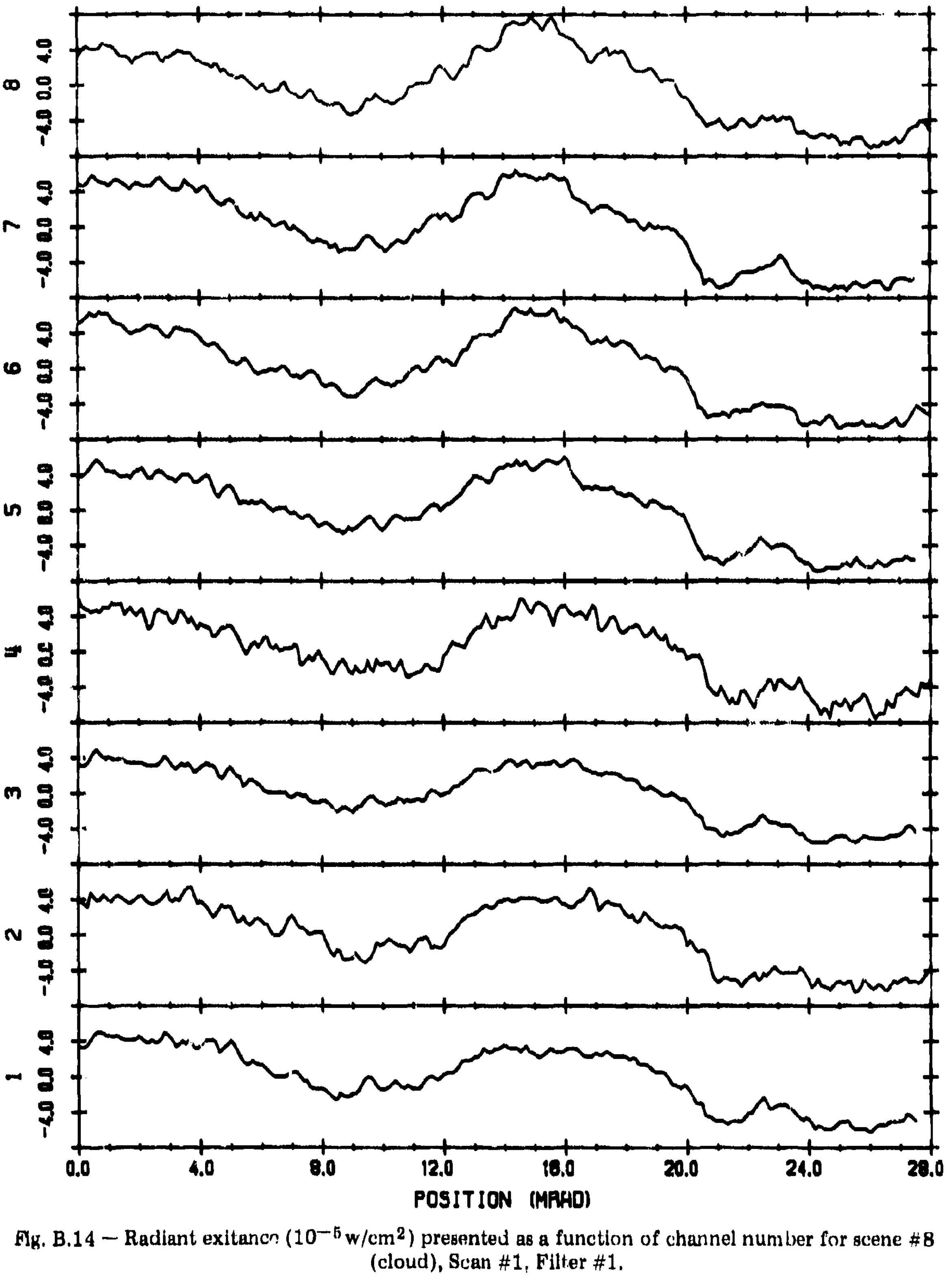

Fig. B.14 — Radiant exitance (10^{-5} w/cm^2) presented as a function of channel number for scene #8 (cloud), Scan #1, Filter #1.

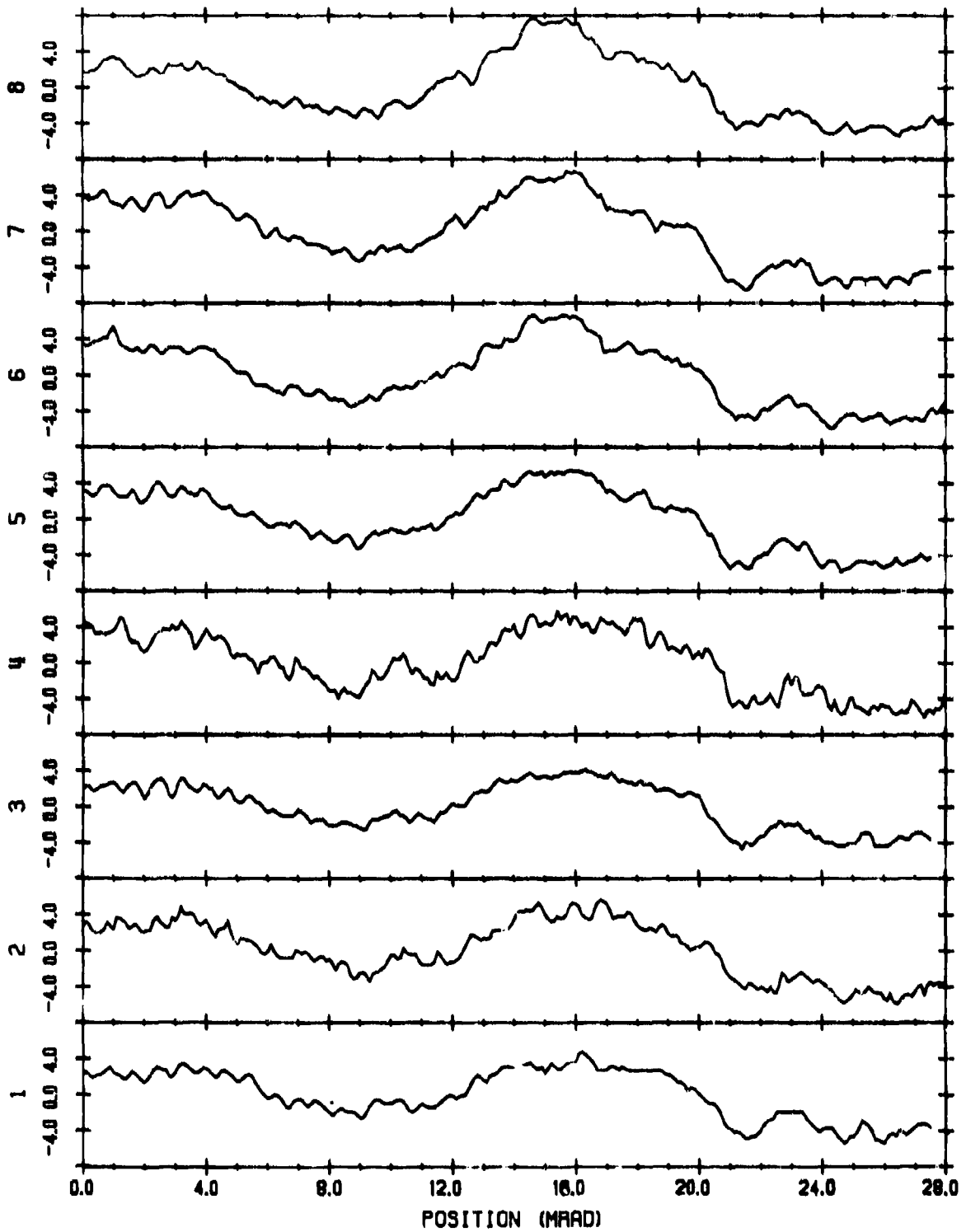

Fig. B.15 – Radiant exitance (10^{-5} w/cm^2) presented as a function of channel number for scene #8 (cloud), Scan #2, Filter #1.

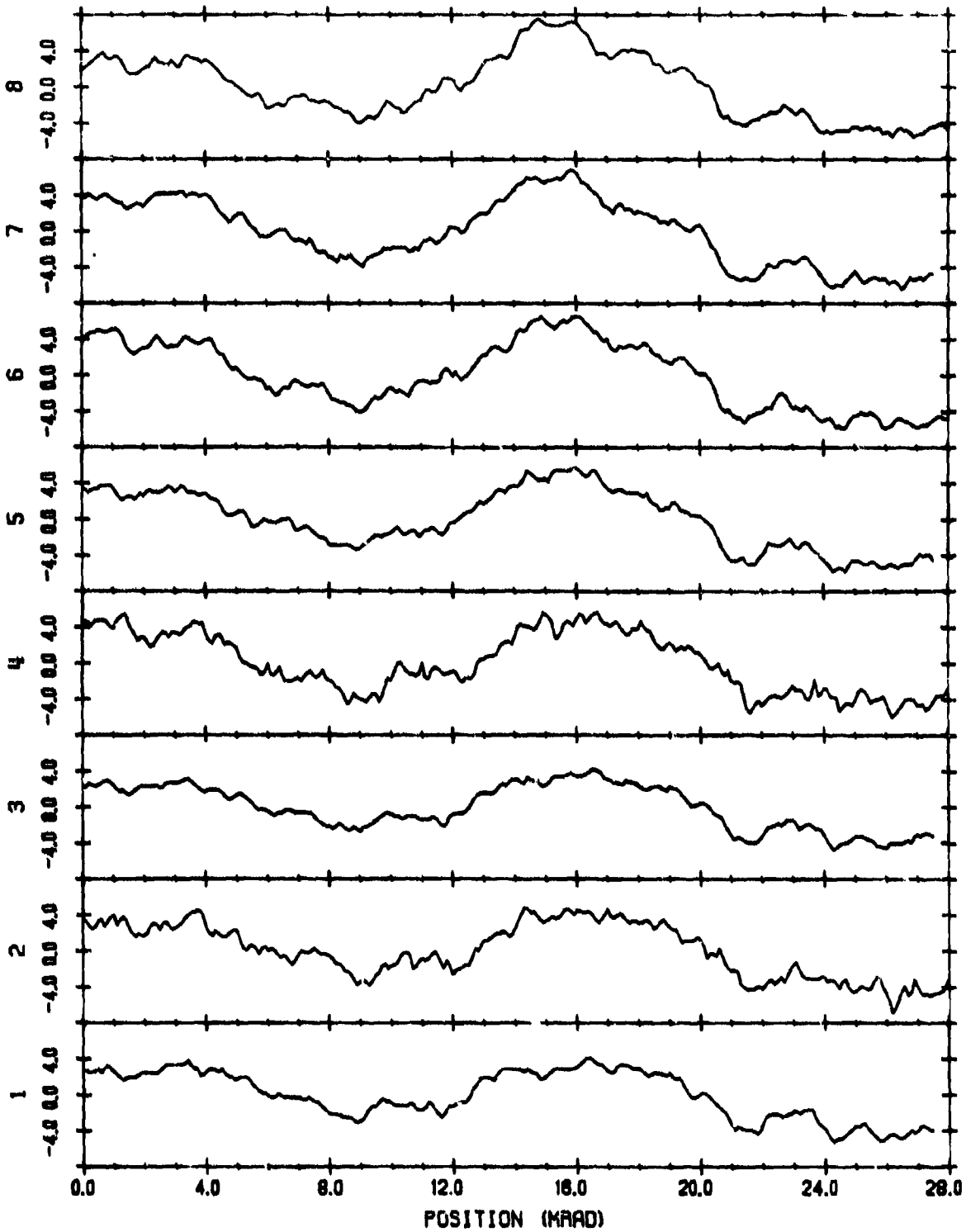

Fig. B.16 — Radiant exitance (10^{-5} w/cm^2) presented as a function of channel number for scene #8 (cloud), Scan #3, Filter #1.

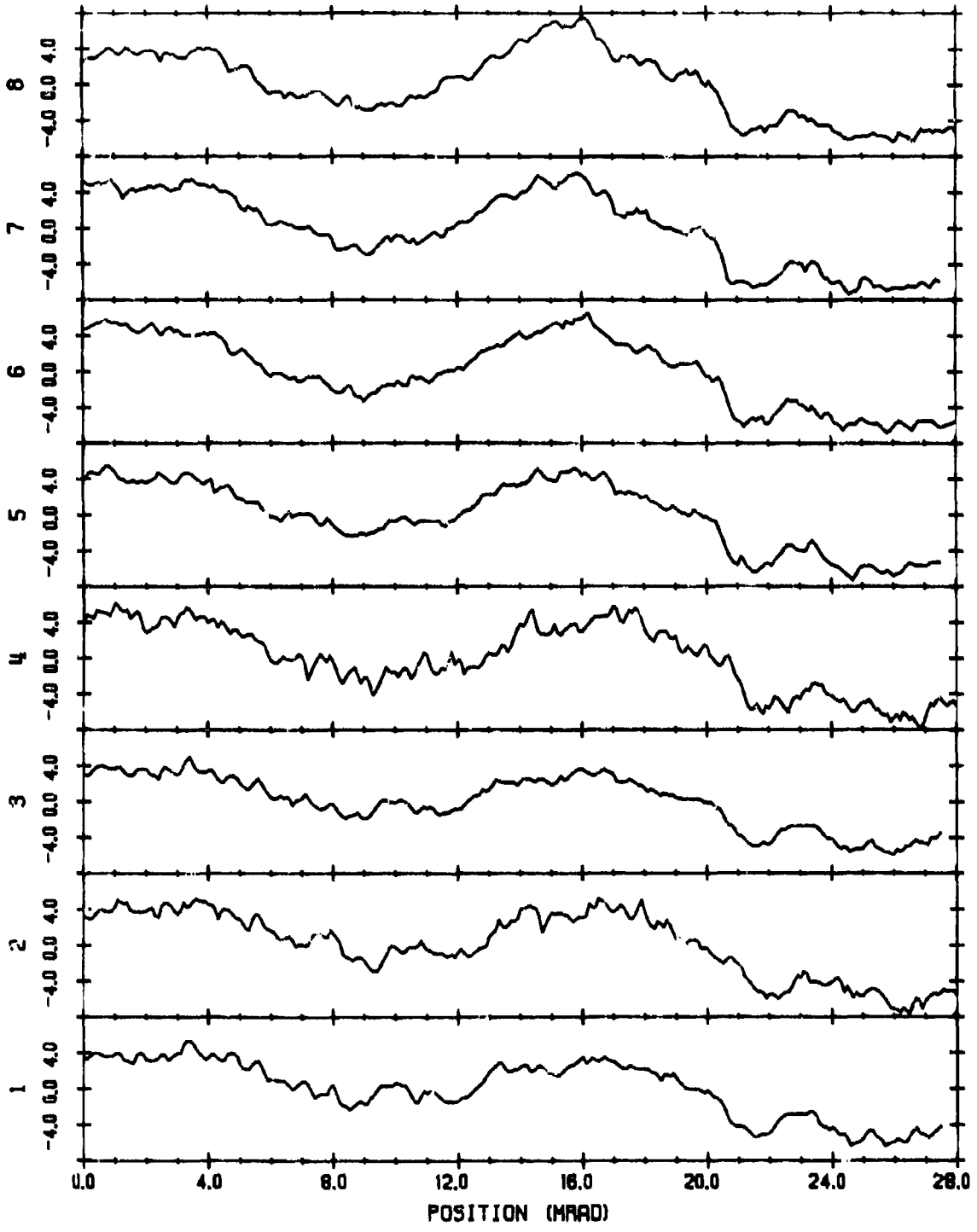

Fig. B.17 — Radiant exitance (10^{-5} w/cm^2) presented as a function of channel number for scene #8 (cloud), Scan #4, Filter #1.

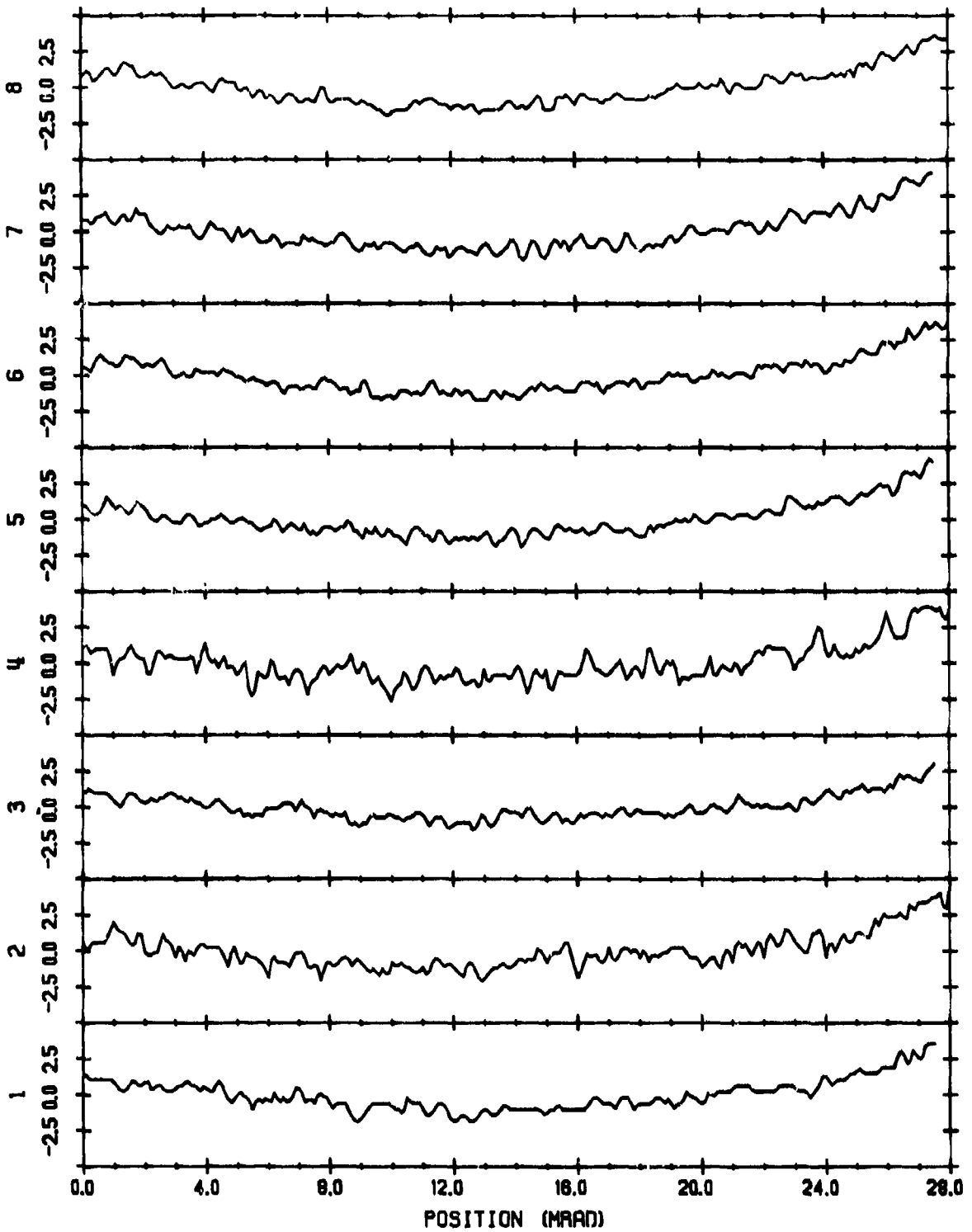

Fig. B.18 — Radiant exitance (10^{-5} w/cm^2) presented as a function of channel number for scene # 11 (cloud), Scan #1, Filter #1.

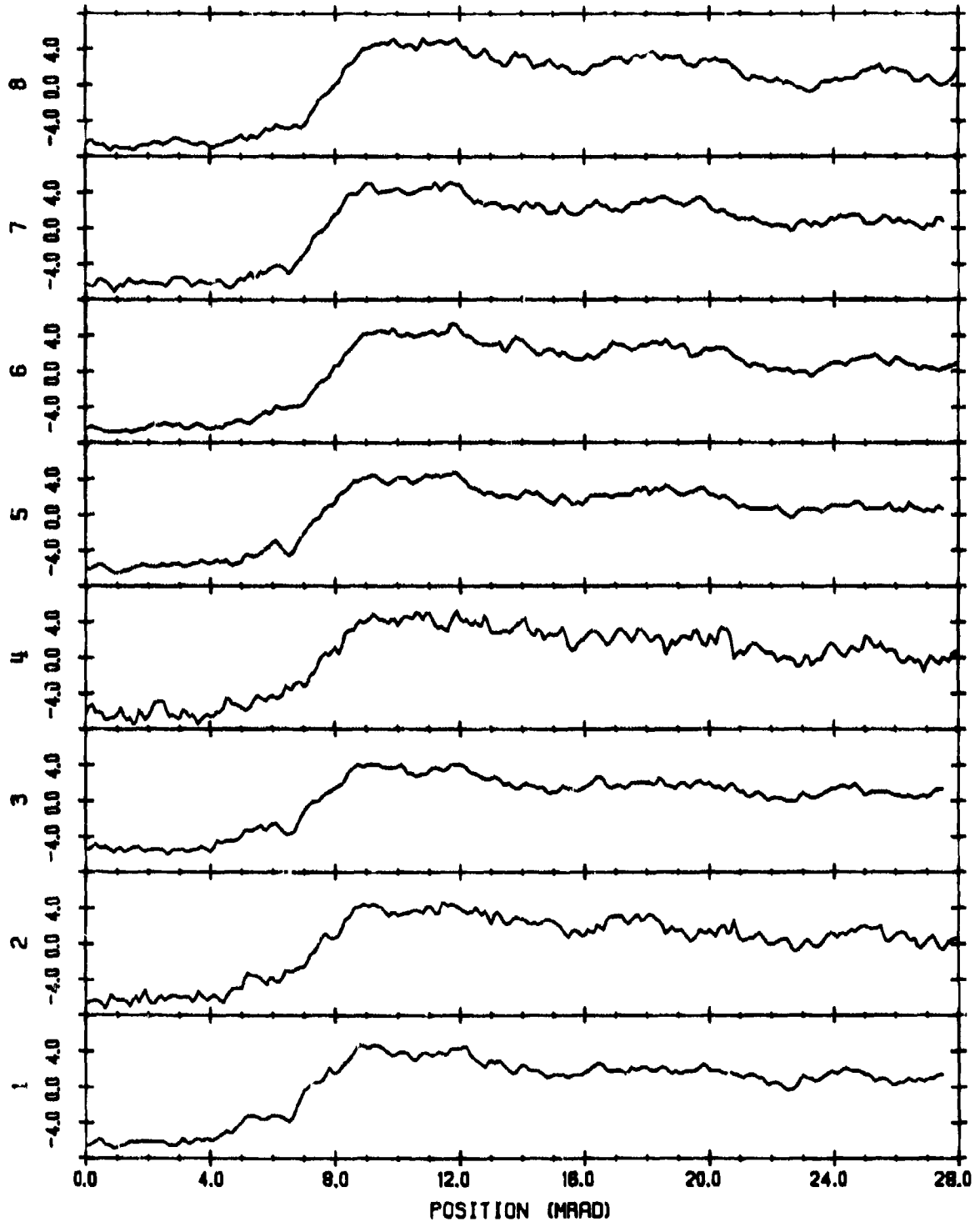

Fig. B.19 — Radiant exitance (10^{-5} w/cm^2) presented as a function of channel number for scene #18 (cloud), Scan #1, Filter #1.

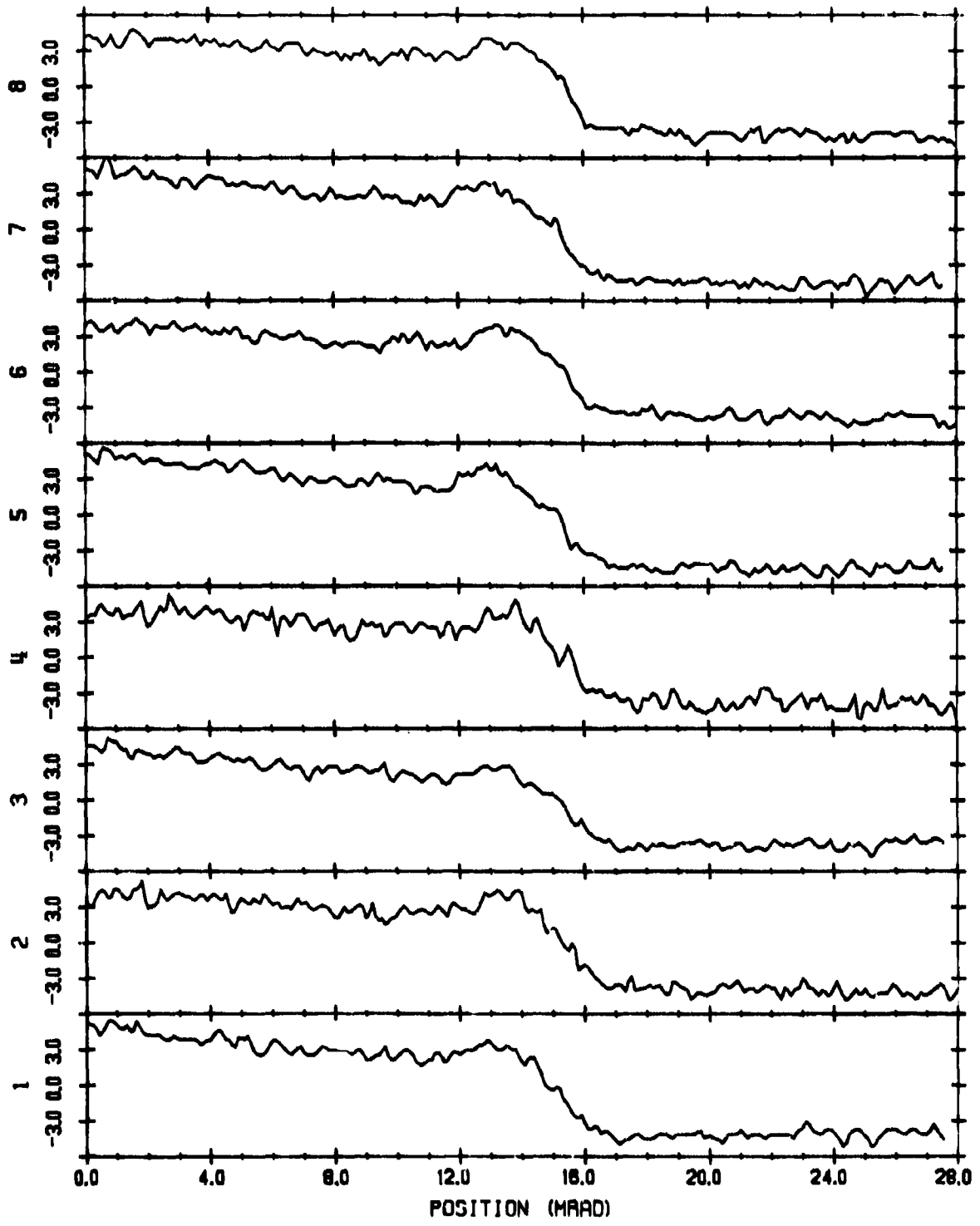

Fig. B.20 — Radiant exitance (10^{-5} w/cm^2) presented as a function of channel number for scene #28 (cloud), Scan #1, Filter #1.

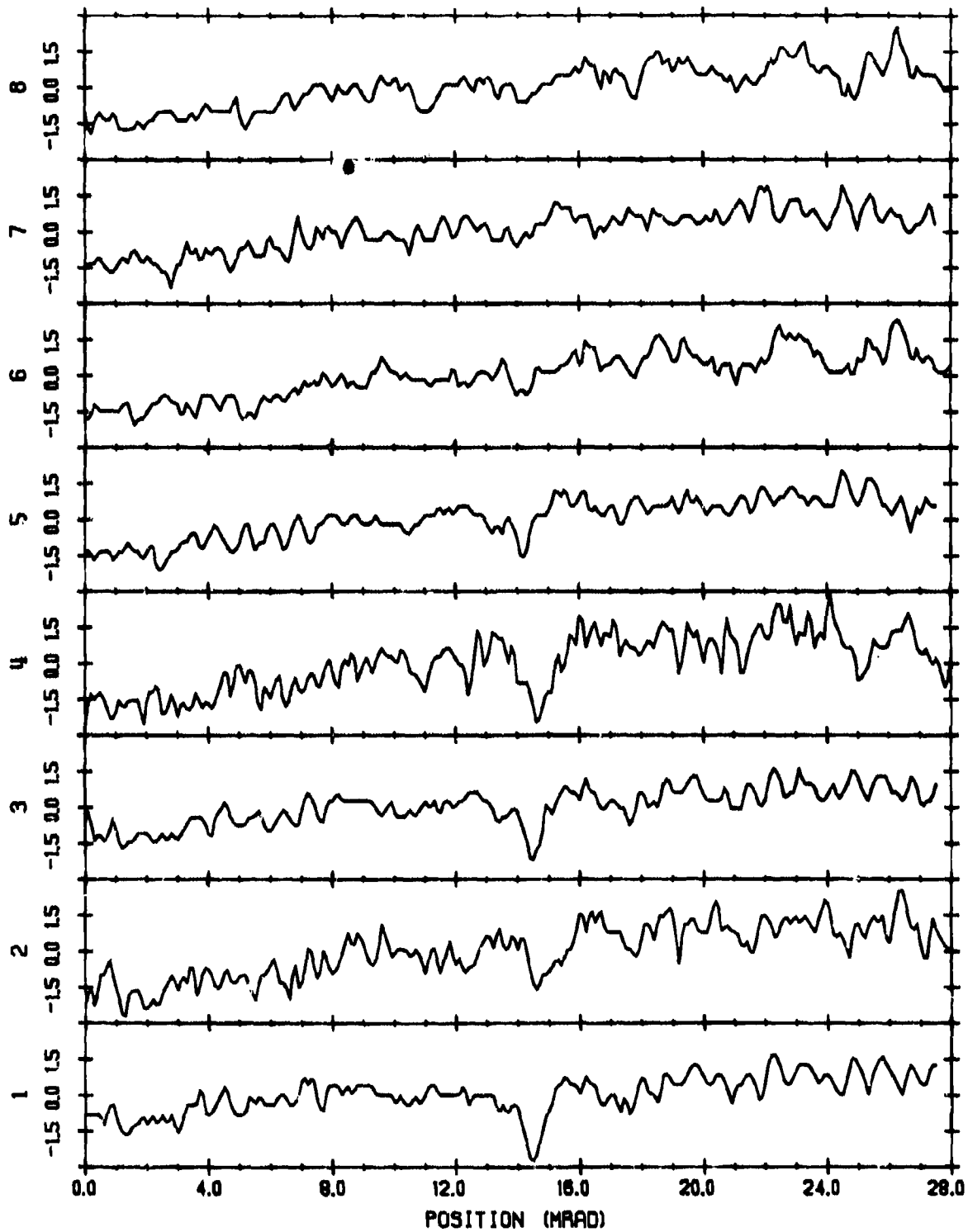

Fig. B.21 — Radiant exitance (10^{-5} w/cm^2) presented as a function of channel number for scene #31 (Microwave Tower), Scan #1, Filter #1. Data are largely dominated by tape noise.

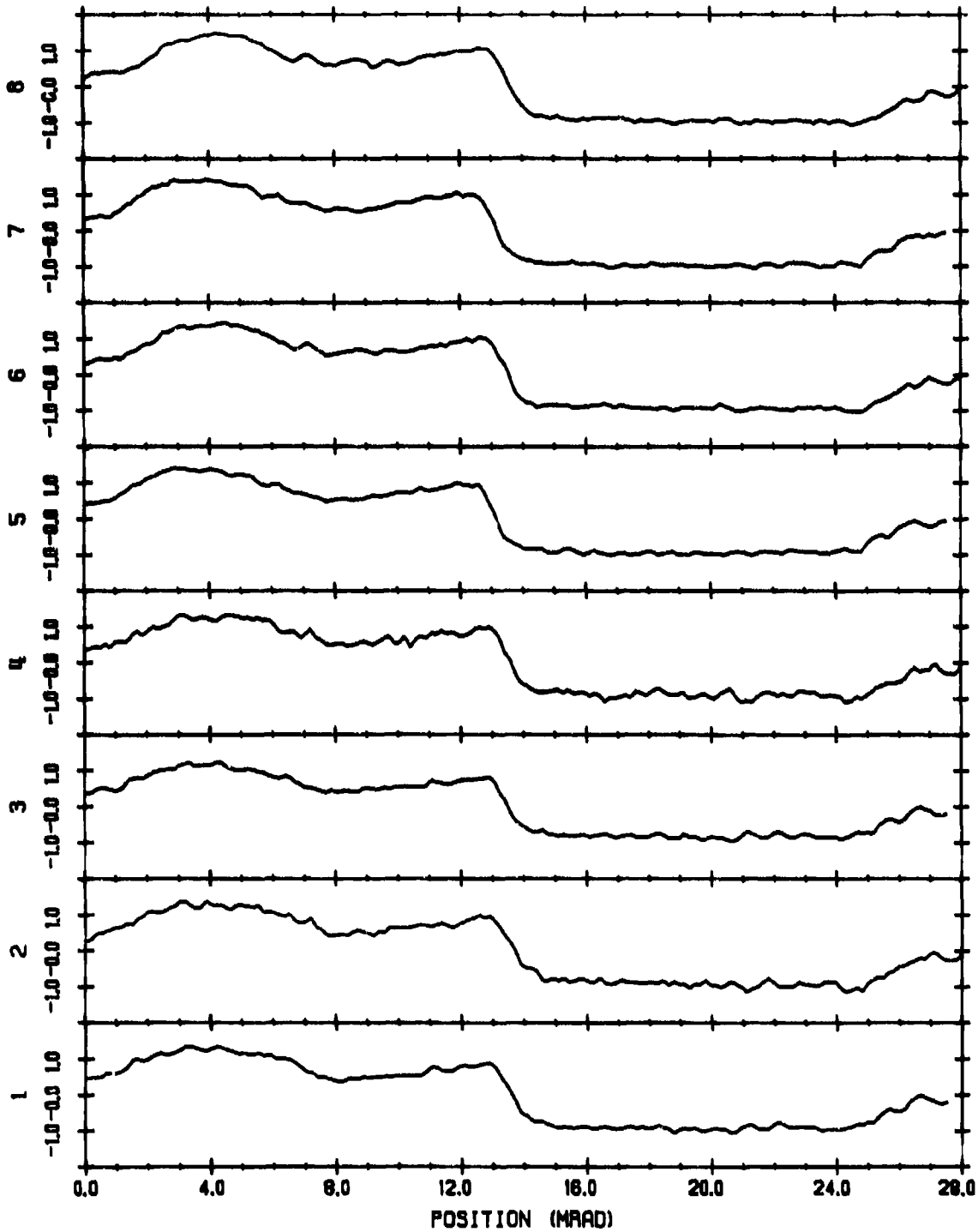

Fig. B.22 — Radiant exitance (10^{-4} w/cm^2) presented as a function of channel number for scene #35 (cloud), Scan #1, Filter #1.

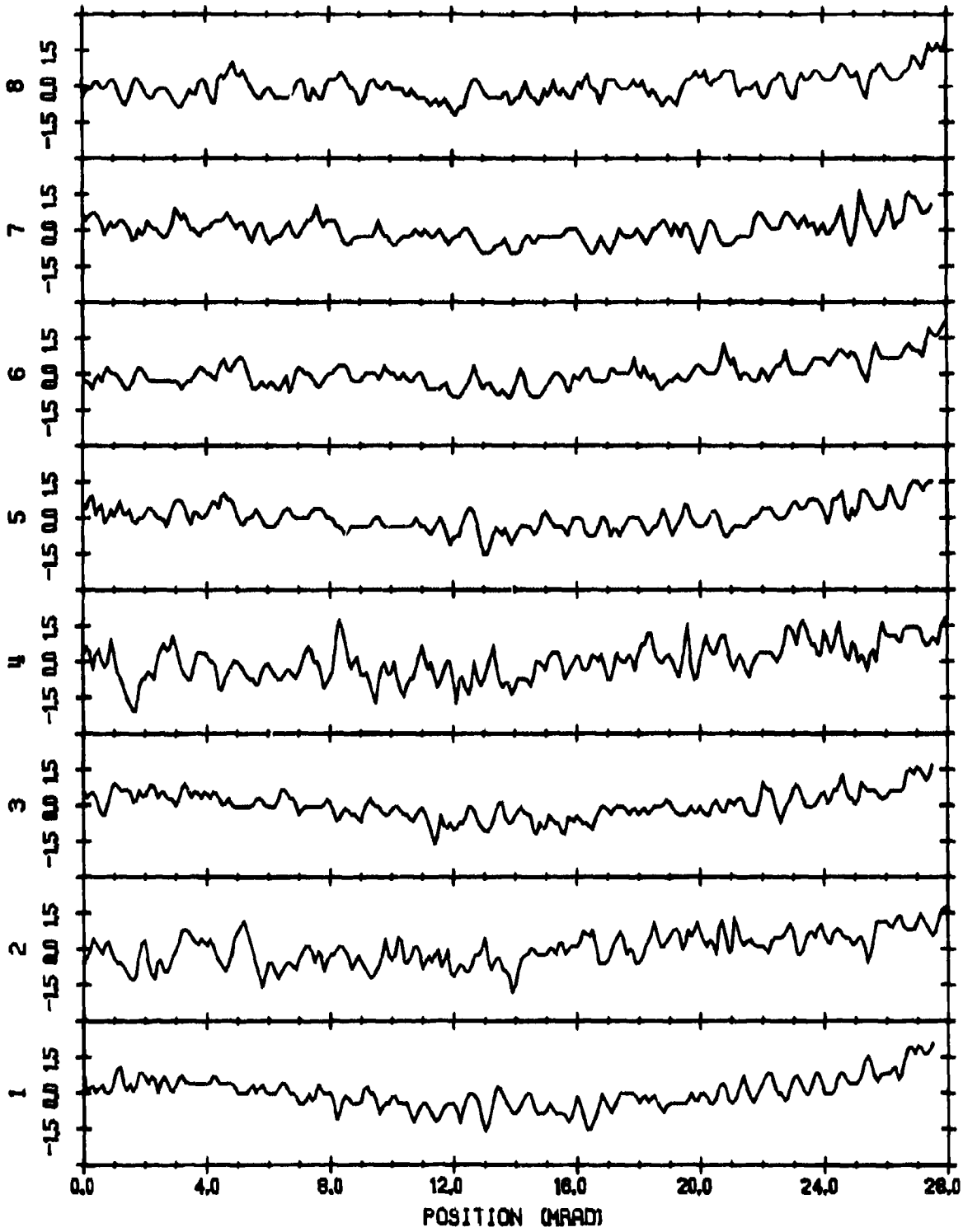

Fig. B.23 — Radiant exitance (10^{-5} w/cm^2) presented as a function of channel number for scene #42 (Cloud deck near horizon), Scan #1, Filter #1. Data are largely dominated by tape noise.

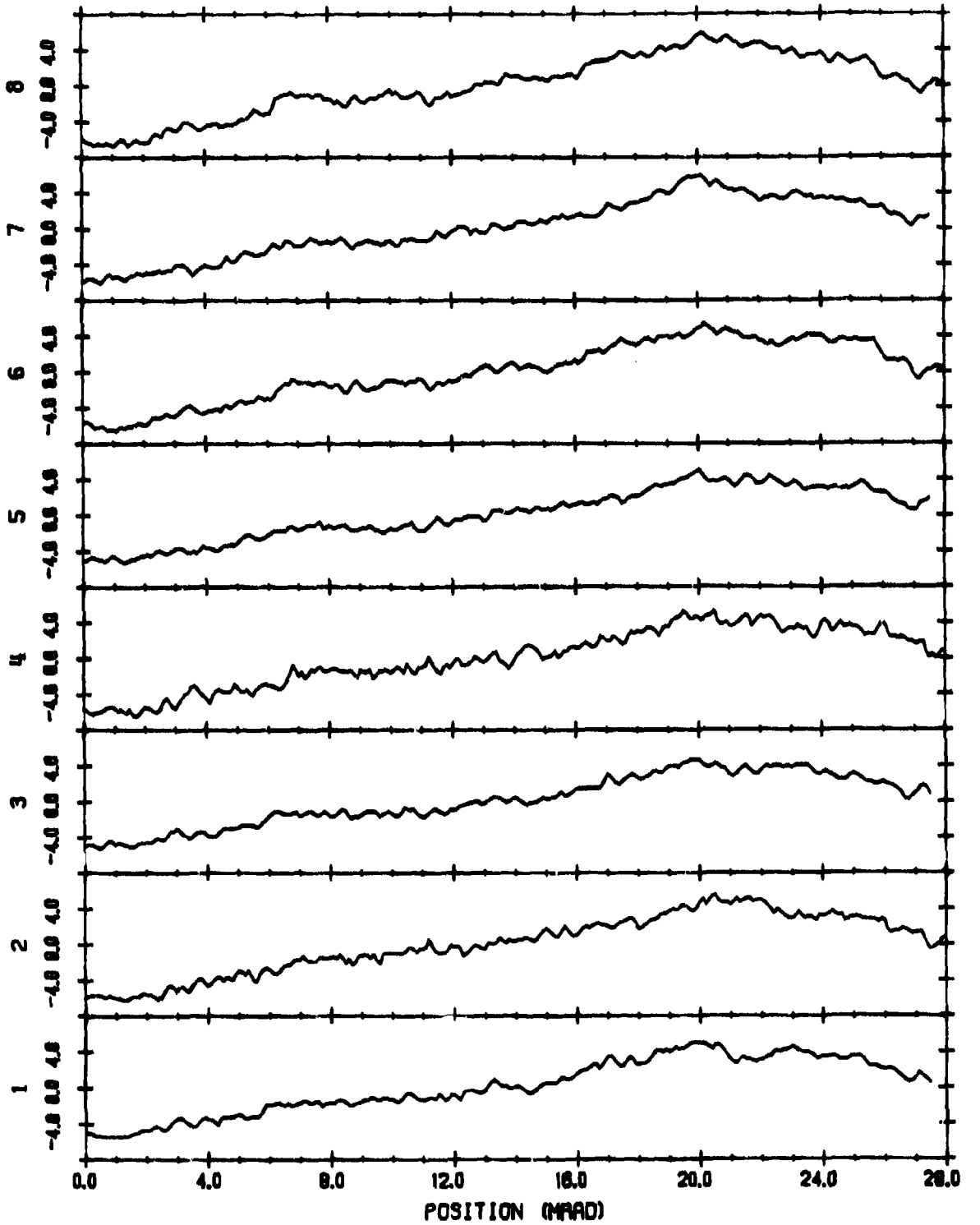

Fig. B.24 — Radiant exitance (10^{-5} w/cm^2) presented as a function of channel number for scene #57 (cloud edge), Scan #1, Filter #1.